

1 **African Smoke Particles Act as Cloud Condensation Nuclei in the Wintertime Tropical**
2 **North Atlantic Boundary Layer over Barbados**

3 Haley M. Royer¹, Mira L. Pöhlker^{2,3,4*}, Ovid Krüger², Edmund Blades^{5,6}, Peter Sealy⁵, Nurun
4 Nahar Lata⁷, Zezhen Cheng⁷, Swarup China⁷, Andrew P. Ault⁸, Patricia K. Quinn⁹, Paquita
5 Zuidema¹, Christopher Pöhlker², Ulrich Pöschl², Meinrat Andreae^{2,10,11} and Cassandra J.
6 Gaston^{1*}

7 ¹Department of Atmospheric Sciences, Rosenstiel School of Marine, Atmospheric, and Earth
8 Science, University of Miami, Miami, FL, United States of America

9 ²Department of Multiphase Chemistry, Max Planck Institute for Chemistry, Mainz, Germany

10 ³Leipzig Institute for Meteorology, Leipzig University, Leipzig, Germany

11 ⁴Experimental Aerosol and Cloud Microphysics Department, Leibniz Institute for Tropospheric
12 Research, Leipzig, Germany

13 ⁵Barbados Atmospheric Chemistry Observatory, Ragged Point, Barbados

14 ⁶Queen Elizabeth Hospital Barbados, Bridgetown, Barbados

15 ⁷Environmental Molecular Sciences Laboratory, Pacific Northwest National Laboratory,
16 Richland, WA, United States of America

17 ⁸Department of Chemistry, University of Michigan, Ann Arbor, MI, United States of America

18 ⁹Pacific Marine Environmental Laboratory, National Oceanic and Atmospheric Administration,
19 Seattle, WA, United States of America

20 ¹⁰Department of Geology and Geophysics, King Saud University, Riyadh, Saudi Arabia

21 ¹¹Scripps Institution of Oceanography, University of California San Diego, La Jolla, California,
22 United States of America

23 *Corresponding Authors:

24 Mira L. Pöhlker: Email: poehlker@tropos.de, Phone: +49 6131 305 7020

25 Cassandra J. Gaston: Email: cgaston@miami.edu, Phone: (305)-421-4979

26

27

28 **Abstract**

29 The number concentration and properties of aerosol particles serving as cloud condensation
30 nuclei (CCN) are important for understanding cloud properties, including in the tropical Atlantic
31 marine boundary layer (MBL) where marine cumulus clouds reflect incoming solar radiation and
32 obscure the low-albedo ocean surface. Studies linking aerosol source, composition, and water
33 uptake properties in this region have been conducted primarily during the summertime dust
34 transport season, despite the region receiving a variety of aerosol particle types throughout the
35 year. In this study, we compare size-resolved aerosol chemical composition data to the
36 hygroscopicity parameter κ derived from size-resolved CCN measurements made during the
37 EUREC⁴A and ATOMIC campaigns from January to February 2020. We observed unexpected
38 periods of wintertime long-range transport of African smoke and dust to Barbados. During these
39 periods, the accumulation mode aerosol particle and CCN number concentrations as well as the
40 proportions of dust and smoke particles increased, whereas the average κ slightly decreased ($\kappa =$
41 0.46 ± 0.10) from marine background conditions ($\kappa = 0.52 \pm 0.09$) when the particles were mostly
42 composed of marine organics and sulfate. Size-resolved chemical analysis shows that smoke
43 particles were the major contributor to the accumulation mode during long-range transport
44 events, indicating that smoke is mainly responsible for the observed increase in CCN number
45 concentrations. Earlier studies conducted at Barbados have mostly focused on the role of dust on
46 CCN, but our results show that aerosol hygroscopicity and CCN number concentrations during
47 wintertime long-range transport events over the tropical North Atlantic are also affected by
48 African smoke. Our findings highlight the importance of African smoke for atmospheric
49 processes and cloud formation over the Caribbean.

50

51 **Introduction**

52 Aerosol particle number, size, hygroscopicity, and chemical mixing state determine cloud
53 droplet formation and, thus, fundamentally affect the radiative properties and lifetime of clouds
54 (Albrecht, 1989; McFiggans et al., 2006; Quinn et al., 2008; Twomey, 1977; Zuidema et al.,
55 2008). Quantifying the effect of aerosols on cloud radiative forcing, however, is still the single
56 largest source of uncertainty in predicting temperature increases associated with climate change
57 (Forster et al., 2021). This uncertainty is especially important to resolve in marine regions where
58 aerosol-cloud interactions are understudied, even though the majority of Earth’s surface is
59 covered by oceans (Carslaw et al., 2013). The existing literature that explores marine aerosol-
60 cloud interactions does so primarily in the mid to high latitudes of the North Atlantic with few
61 studies focusing in tropical latitudes where shallow cumulus clouds form (Allan et al., 2008;
62 Behrenfeld et al., 2019; Klingebiel et al., 2019; Rauber et al., 2007; Sorooshian et al., 2020).
63 Shallow cumulus clouds are important for Earth’s climate as they are one of the most
64 geographically pervasive cloud types and can influence Earth’s radiative budget by reflecting
65 incoming radiation over the low-albedo ocean surface.

66 Aerosol research conducted in the tropical Atlantic has focused largely on the long-range
67 transport of mineral dust from North Africa in the summertime. Long-range African dust
68 transport occurs when emitted desert dust is lofted above the marine boundary layer (MBL) into
69 the Saharan Air Layer (SAL) and is propagated westward (Carlson & Prospero, 1972). As dust is
70 transported westward, it can mix into the underlying moist MBL and deposit into the Atlantic
71 Ocean and Caribbean Sea as well as Western Atlantic land masses such as South America, the
72 Caribbean islands, and North America (Barkley et al., 2019; Carlson & Prospero, 1972; Prospero et
73 al., 1981, 2020). Some studies have attempted to understand the effects of long-range transported

74 dust on cloud droplet formation and water uptake with varying results depending on the degree
75 of aging that dust experiences during transport (Allan et al., 2008; Denjean et al., 2015;
76 Kristensen et al., 2016; Rosenfeld et al., 2001; Wex et al., 2016). However, these studies provide
77 conflicting results on whether dust particles are hygroscopic and numerous enough to
78 appreciably impact CCN concentrations in the tropical Atlantic. Due to the annual oscillation of
79 the intertropical convergence zone (ITCZ), dust transport also exhibits a seasonality in terms of
80 its geographic extent (Adams et al., 2012; Chin et al., 2014; Prospero & Lamb., 2003; Prospero, 1968;
81 Prospero & Mayol-Bracero, 2013; Yu et al., 2019; Zuidema et al., 2019). However, marine shallow
82 cumulus clouds form year-round in the tropical Atlantic regardless of dust transport. Thus, it is
83 important to focus on aerosol characteristics across a full seasonal cycle to obtain a thorough
84 understanding of the role aerosols play on cloud formation in the tropical Atlantic (McCoy et al.,
85 2022).

86 Few studies have attempted to fully understand which aerosols are the most prominent
87 CCN during both the boreal summer (when dust concentrations are at a maximum) and boreal
88 winter (when dust concentrations are at a minimum) in the tropical North Atlantic MBL. African
89 smoke is one particle type that may be important for CCN activation in the tropical North
90 Atlantic, yet has been understudied at dust receptor sites like Barbados (Wex et al., 2016). In
91 contrast to dust, previous research has shown that smoke particles are an important source of
92 CCN (Edwards et al., 2021; Latham et al., 2013; Pierce et al., 2007; Spracklen et al., 2011) with
93 some research showing that smoke particles can activate at supersaturations as low as 0.05%
94 (Rogers et al., 1991).

95 There are a number of reasons that explain why smoke particles can be effective CCN.
96 Smoke particles are often complex mixtures of both organic and inorganic components that

97 change compositionally and morphologically during their residence time in the atmosphere
98 (Cappa et al., 2020; Hodshire et al., 2019; Konovalov et al., 2021; Reid et al., 2005; Wu et al.,
99 2021). Smoke properties may also vary between fires depending on fuel type and moisture,
100 combustion phase, wind conditions, etc. (Andreae, 2019; Miles et al., 1995; Reid et al., 2005). In
101 general, smoke particles are often found in the accumulation mode of the aerosol size
102 distribution and primarily contain particulate organic matter, black carbon, and inorganic
103 components including potassium chloride salts (Reid et al., 2005). Upon emission, smoke can
104 undergo chemical processing through photochemical and heterogeneous reactions, including the
105 loss of chloride and acquisition of sulfate and nitrate, creating potassium sulfate compounds in
106 smoke that are often used as tracers of aged smoke and can affect the hygroscopicity of smoke
107 particles (Capes et al., 2008; Hennigan et al., 2010, 2011; Reid et al., 2005; Zauscher et al.,
108 2013). Chemical processing can also lead to morphological changes as the condensation of
109 gaseous compounds and multiphase processes with aqueous compounds can result in the growth
110 and sphericity of smoke particles, which in turn can affect the CCN properties of smoke particles
111 (Abel et al., 2003; Giordano et al., 2015; Reid et al., 1998; Zhang et al., 2008). The variations in
112 the chemical and physical properties of emitted smoke particles as well as the changes these
113 properties can undergo in transit make it difficult to predict the ability of smoke particles to act
114 as CCN.

115 In this study, we investigated the relationship between submicron aerosol composition
116 and CCN in the tropical North Atlantic MBL during marine background conditions and
117 conditions affected by long-range continental aerosol transport of smoke and dust particles
118 (henceforth referred to as “CAT” conditions). To perform this work, we collected aerosol
119 samples and size-resolved CCN data from January to February 2020 at the Barbados

120 Atmospheric Chemistry Observatory (BACO) during the Elucidating the Role of Clouds–
121 Circulation Coupling in Climate/Atlantic Tradewind Ocean-Atmosphere Mesoscale Interaction
122 Campaign (EUREC⁴A/ATOMIC) campaigns (Quinn et al., 2021; Stevens et al., 2021).
123 Conducting this research during the boreal winter provided a unique opportunity to explore
124 aerosol-cloud interactions in meteorological conditions different from those that are typically
125 studied in the tropical North Atlantic. Dust primarily arrives to Barbados during the summer
126 months with peaks in June and July (Zuidema et al., 2019). As a result, dust receptor sites in
127 Barbados have historically been used to compare CAT and marine background conditions during
128 the boreal summer. During the winter, the southward shift of the ITCZ directs African dust to
129 South America, resulting in a decrease in dust concentrations over Barbados during the winter
130 months with days in December and January sometimes receiving no dust at all (Prospero, 1968;
131 Prospero et al., 2014; Prospero & Lamb, 2003; Prospero & Mayol-Bracero, 2013). However, during the
132 EUREC⁴A/ATOMIC campaigns, we observed anomalous wintertime transport of African
133 aerosols to Barbados, which provided novel sampling conditions to study the effects of various
134 aerosol types on cloud droplet formation. Specifically, we were able to explore how the addition
135 of continental aerosols like mineral dust and smoke particles to background marine aerosols
136 consisting of organics, sulfates, and sea salt affects CCN activity. This allowed us to compare the
137 impact of ocean-derived vs. long-range transported aerosol on water uptake properties and CCN
138 concentrations. We conclude this manuscript by discussing the importance of our findings for
139 cloud formation in the tropical North Atlantic.

140 **Methods**

141 Measurement Site and Sampling Period

142 Aerosol samples and size-resolved CCN data were collected at the Barbados
143 Atmospheric Chemistry Observatory (BACO) on Ragged Point during the EUREC⁴A and
144 ATOMIC field campaigns from January 20, 2020 -February 20, 2020 (Quinn et al., 2021;
145 Stevens et al., 2021). Ragged Point (13° 6' N, 59° 37' W), a prominence on Barbados' east coast,
146 is an ideal location for studying the impact of long-range African aerosol transport on aerosol-
147 cloud interactions as it is situated on the most easterly island in the Caribbean and is exposed to
148 the steady easterly trade winds. Thus, the east coast of the island is subject to little anthropogenic
149 aerosol influence from local islands to the west (Prospero et al., 2005; Savoie et al., 2002).
150 Further, the island is at a latitude coinciding with the outflow of African aerosols such as mineral
151 dust (Carlson & Prospero, 1972; Prospero, 1968) and smoke particles (Archibald et al., 2015) as well
152 as tropical marine cumulus clouds (Stevens et al., 2016).

153 Air Mass Origins

154 During the sampling period, air masses of varying compositions were observed at Ragged
155 Point. To determine the origin of these air masses, 150 h back trajectories were generated every 6
156 h at heights of 500, 1000, and 1500 m throughout the campaign using the NOAA Hybrid Single
157 Particle Lagrangian Integrated Trajectory (HYSPLIT) model calculated using model vertical
158 velocity and meteorology from the National Center for Environmental Prediction (NCEP) 1-
159 degree Global Data Assimilation System (GDAS) (Rolph et al., 2017; Stein et al., 2015).

160 Dust Concentration

161 To collect aerosols, BACO is equipped with a high-volume sampler and an isokinetic
162 aerosol inlet on top of a 17 m tall tower situated on a 30 m bluff along the coast at Ragged Point.
163 Daily dust mass concentrations were determined from filter-based measurements (Prospero et al.,

164 2021; Zuidema et al., 2019) using a high-volume air sampler pumping at a rate of approximately
165 0.7 m³/min across a 20 cm x 25 cm cellulose Whatman-41 (W-41) filter with a nominal 20 µm
166 pore size. W-41 filters were chosen for this analysis as they allow high flow rates and yield a
167 collection efficiency of 95% or better for dust (Kitto & Anderson, 1988) and submicron aerosols
168 (Pszenny et al., 1993). Upper particle diameter limits for W-41 filters are approximately 80-100
169 µm or greater (Barkley et al., 2021). After aerosol collection, the filters are washed with milli-q
170 water three times to remove soluble material then placed in a furnace and combusted at 500°C
171 for about 12 h (i.e., overnight). Procedural blanks are also collected by placing a filter in the
172 sampler for 15 minutes without turning on the pump. The resulting ash mass from a sample
173 minus the mass of a filter blank is the gross ash weight, which is then adjusted by a factor of 1.3
174 to convert the ash weight to a mineral dust concentration. Previous research has confirmed the
175 validity of this method for determining dust mass concentrations through chemical analysis of
176 dust ash determined from filters collected in Barbados, crustal abundance, and soil dust
177 composition (Zuidema et al., 2019). A correction factor of 1.3 is applied to the calculated dust
178 concentrations to account for dust components such as bound water or soluble ions that are lost
179 during the heating process (Prospero, 1999; Zuidema et al., 2019).

180 Aerosol Chemical Composition

181 Aerosol particles were sampled at ambient relative humidity (RH) through an isokinetic
182 aerosol inlet and collected using a three-stage microanalysis particle sampler (MPS-3, California
183 Measurements, Inc.), which samples particles from diameters of 5.0-2.5 µm (stage 1), 2.5 µm –
184 0.7 µm (stage 2), and <0.7 µm (stage 3). For each set of samples (1 set including 1 sample from
185 each stage of the MPS), the MPS was run for 45 min at 2 L/min flow starting at approximately
186 9:30 local time or 13:30 coordinated universal time (UTC). Meteorological data from a local

187 station was also used to manually check that wind direction fell between 335° and 130° and wind
188 speeds were greater than 1 m/s during all sampling periods. Sampling during these wind
189 conditions ensures that only air from the open ocean was sampled rather than local,
190 anthropogenically-influenced air.

191 To determine aerosol chemical composition, particles were deposited onto carbon-
192 coated copper grids (Ted Pella, Inc.) that were later analyzed at the Pacific Northwest National
193 Laboratory using computer-controlled scanning electron microscopy coupled with energy
194 dispersive x-ray spectroscopy (CCSEM/EDX; Quanta 3D) to determine the elemental
195 composition of individual particles. We also collected samples on silicon wafers (Ted Pella, Inc.)
196 which were analyzed with CCSEM/EDX to confirm the validity of the carbon measurements on
197 the carbon-coated copper grids. Here, we focus only on the submicron particle population which
198 exerts a greater influence on CCN number concentrations and is more sensitive to chemical
199 changes that affect its hygroscopicity. Thus, for this study we focus primarily on data from stage
200 3 of the MPS, representing <0.7 μm diameter particles.

201 CCSEM/EDX is a valid method for determining size-resolved chemistry of the aerosol
202 loading as CCSEM excels in calculating particle size by imaging individual aerosols while EDX
203 provides the relative abundances for elements of interest (Tomlin et al., 2021). Percent
204 composition threshold values of 1% were used to ensure the presence of elements detected by the
205 EDX. Single-particle analysis using CCSEM/EDX was limited to 16 elements found in common
206 aerosols such as dust, sea salt, and smoke particles: carbon (C), nitrogen (N), oxygen (O),
207 sodium (Na), magnesium (Mg), aluminum (Al), silicon (Si), phosphorus (P), sulfur (S), chlorine
208 (Cl), potassium (K), calcium (Ca), vanadium (V), manganese (Mn), iron (Fe), and nickel (Ni).
209 The EDX peak for Cu is heavily influenced by the background signal from the Cu grid and is

210 excluded from analysis. Samples collected on Si substrates confirmed the validity of the C signal
211 in analyzed particles, as the carbon coating on the Cu substrates has the potential to generate a
212 background signal as well. An excess of 1000 particles were analyzed in each sample. Due to
213 size limitations of the CCSEM, only particles with diameters $>0.1 \mu\text{m}$ were analyzed. Data
214 products from CCSEM/EDX analysis were then analyzed in MATLAB (ver 9.6.0; The
215 Mathworks, Inc.) using a K-means clustering algorithm (Ault et al., 2012; Shen et al., 2016). The
216 algorithm operates by generating categories of similar particles (clusters) based on the presence
217 and intensity of elemental peaks in individual single-particle EDX spectra. These clusters are
218 then assigned to particle types based on their size, morphology, characteristic EDX spectra, and
219 existing literature. A more thorough explanation of the k-means clustering algorithm and particle
220 identification process including the plots used to perform particle identification (Figure S1) is
221 provided in the Supporting Information (SI).

222 Size-Resolved CCN Measurements and Data Analysis

223 To determine the size-resolved CCN activity of aerosol particles during the sampling
224 period, we used a continuous-flow streamwise thermal gradient CCN counter (CCNC, model
225 CCN-100, DMT, Longmont, Co, USA; (Roberts & Nenes, 2005; Rose et al., 2008)) combined with
226 a differential mobility analyzer (DMA, modified model M, Grimm Aerosol Technik, Ainring,
227 Germany) and condensation particle counter (CPC, model 5412, Grimm Aerosol Technik). The
228 method is described in detail in Pohlker et al. (2016). Flows for the size-resolved CCN set-up
229 included a sheath:sample flow ratio of 10 for the CCN counter (sample flow rate of 0.5 L/min), a
230 sheath flow of 8 L/min for the DMA, and a sample flow of 0.6 L/min for the CPC. Upon entering
231 the system, the sampled air was dried using a condensation drier to maintain a relative humidity
232 (RH) between 20 and 30% and to ensure reliable hygroscopicity measurements. After drying, the

233 particles passed through a DMA which selected particles with a diameter (D) between 20 and
234 245 nm. The monodisperse aerosol-laden flow was then split between the CCNC and CPC.
235 Inside the CCNC, the particles were subjected to supersaturations (S) of 0.09, 0.16, 0.24, 0.43,
236 and 0.74 %.

237 Calibrations of the CCNC supersaturations were performed according to the method
238 described in Rose et al. (2008) by generating and size-selecting ammonium sulfate particles that
239 were analyzed by the CCNC set to a designated temperature gradient as well as a CPC to
240 measure total condensation nuclei (CN) values. Plots comparing CCN/CN and dry particle
241 diameter were then used to determine the diameter at which 50% of the particles in an aerosol
242 population activate as CCN at a particular S , also called the critical activation diameter (d_{50}). D_{50}
243 values were then used to determine supersaturation. Supersaturations were plotted against the
244 designated temperature at the calculated supersaturation. The resulting plot provided a linear
245 curve that could be used to adjust the supersaturation shown by the instrument to the actual value
246 of the column supersaturation. After calibrating, S values averaged 0.08, 0.15, 0.23, 0.41, and
247 0.71%.

248 For ambient sampling, particles that activate as CCN at each S and D are counted in the
249 CCNC as CCN, while all particles of a selected D are counted in the CPC to determine the total
250 aerosol concentration of particles at each D . By scanning D at a given value of S , measurements
251 from the CPC and CCNC are then used to generate an activation curve used to calculate the d_{50} .
252 These values, along with the particle number size distribution determined by an SMPS (SMPS,
253 Grimm model 5420 with CPC 3772) operating independently of the CCNC set-up, are then used
254 to calculate the effective hygroscopicity parameter κ using equation (1) according to the κ -
255 Köhler model (Petters & Kreidenweis, 2007):

256
$$\kappa = \frac{4A^3}{27D_p^3 \ln^2 S_{\text{crit}}} \quad (1)$$

257 where D_p is the dry particle diameter, S_{crit} is the supersaturation set by the CCN counter, and A is
258 the Kelvin term calculated from equation (2):

259
$$A = \frac{4\sigma M_w}{RT\rho_w} \quad (2)$$

260 Where σ is the surface tension ($\sigma=0.072 \text{ J/m}^2$), R is the universal gas constant, M_w is the
261 molecular weight of water, and ρ_w is the density of water. In the κ -Köhler model, higher values
262 of κ indicate a more hygroscopic particle that is more efficient at taking up water and can
263 activate as CCN at lower S .

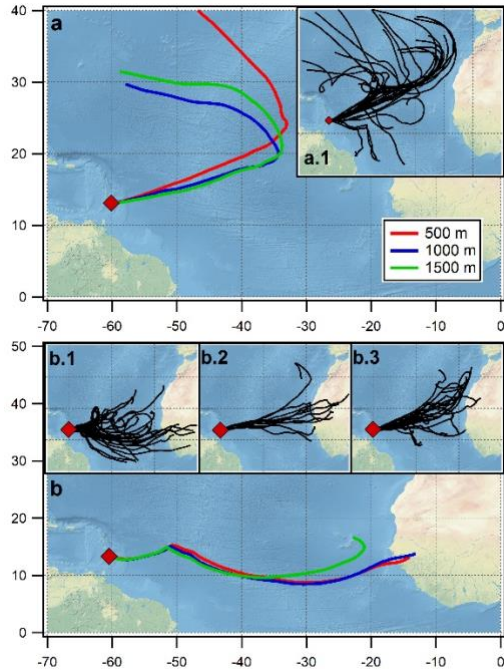
264 **Results and Discussion**

265 In this section we will show that, upon arrival of co-transported dust and smoke, smoke
266 originating from fires in the African Sahel dominate the accumulation mode particle population
267 in the tropical North Atlantic MBL, which results in an increase in CCN number concentration.
268 Though dust and smoke are both transported to the region, smoke dominates the accumulation
269 mode number concentration by an order of magnitude compared to dust. These findings are
270 supported by data products from dust mass concentrations, size-resolved hygroscopicity, single
271 particle data (CCSEM-EDX), and air mass history (NOAA'S HYSPLIT model), which all
272 complement one another and provide unique insights into the aerosol sources, their single
273 particle composition, and their effects on cloud droplet activation.

274 Air Mass Characteristics during the EUREC⁴A and ATOMIC Campaigns

275 To confirm the origins of the various air masses sampled, we performed back trajectory
276 analysis throughout the campaign using NOAA'S HYSPLIT model (Figure 1) and quantified

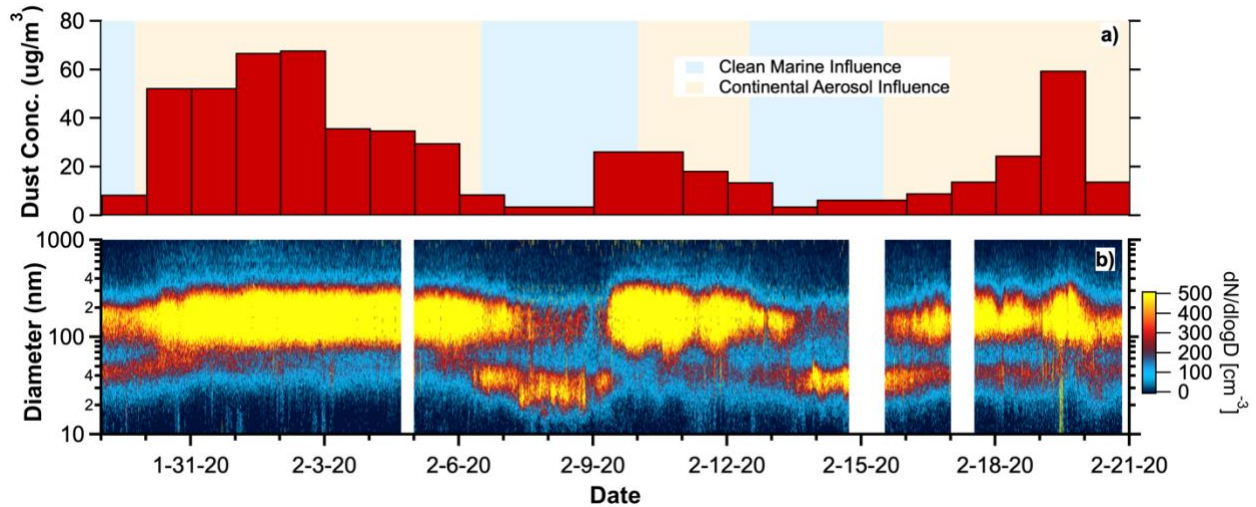
277 dust mass concentrations (Figure 2a). Results of these two analyses show that Barbados was
278 influenced by two types of air masses during the sampling period: air masses that, over the
279 course of 6 days, do not pass over land (referred to as clean marine conditions), and air masses
280 that have passed over the African continent (referred to as continental aerosol transport (CAT)
281 events). Back trajectory analysis was not conducted for time periods longer than 6 days, which
282 introduces the possibility that marine air masses could have been influenced by European
283 outflow as well. Figure 1 shows that during periods with low dust mass concentrations and a
284 bimodal size distribution, air masses originated from the remote Atlantic Ocean at higher
285 latitudes with no land contact over 6 days. During time periods with high dust mass
286 concentrations, air masses originated from continental Africa. Figure 2a shows that the total
287 mass concentration of dust particles correlates very well with the arrival of air masses originating
288 from Africa. During time periods when dust concentrations were low, the particle loading has a
289 bimodal size distribution characteristic of clean marine air masses (Figure 2b; Ault et al., 2013;
290 Hoppel et al., 1986; O'Dowd et al., 2004). Upon the increase in dust mass concentrations, the
291 submicron particle size distribution becomes unimodal and the smallest Aitken size mode is
292 negligible, suggesting that long-range transported (LRT) particles are either dominant over the
293 background marine particle loading or that smaller Aitken mode particles are coagulating onto
294 larger LRT continental aerosols to form a unimodal accumulation mode (Tomlin et al., 2021).



295

296 **Figure 1:** HYSPLIT back trajectories at Ragged Point, Barbados (red diamond) for the
 297 EUREC⁴A/ATOMIC field campaign. (a) Back trajectories for 2020/2/8 18:00 UTC at heights of
 298 500 m (red), 1000 m (blue), and 1500 m (green) exemplify air mass origins during clean marine
 299 sampling conditions. Subplot a.1 shows all back trajectories from clean marine sampling
 300 conditions collected at 6 h intervals with a release altitude of 1000 m from 2020/1/29 0:00 –
 301 2020/1/29 12:00, 2020/2/6 12:00 – 2020/2/9 18:00 and 2020/2/12 12:00 – 2020/2/15 6:00 UTC.
 302 (b) Back trajectories for 2020/2/2 18:00 UTC at 500 m, 1000 m, and 1500 m exemplify air mass
 303 origins during CAT conditions. The subplots, b.1, b.2, and b.3 show all back trajectories for 3
 304 time periods during which continental aerosols were sampled: b.1) 2020/1/29 18:00 – 2020/2/6
 305 6:00, b.2) 2020/2/10 0:00 – 2020/2/12 6:00, and b.3) 2020/2/15 12:00 – 2020/2/20 18:00 UTC.
 306 Trajectories for b subplots were also collected at 6 h intervals with a release altitude of 1000 m.

307



308

309 **Figure 2** – Temporal evolution of (a) dust mass concentrations determined from bulk aerosol
 310 filter samples and (b) submicron aerosol particle size distributions determined with an SMPS.
 311 Time for both plots is given in UTC (-4 h local Atlantic Standard Time). Color shading in (a)
 312 represents continental aerosol influence (orange shading) and clean marine influence (b) as
 313 determined by NOAA HYSPLIT back trajectories calculated at Ragged Point.

314

315 Single Particle Aerosol Composition

316 CCSEM/EDX analysis from the EUREC⁴A and ATOMIC campaigns revealed the presence
 317 of several particle types with distinct chemistries and morphologies in the submicron aerosol
 318 loading (Ault et al., 2014; Behnke et al., 1997; Gaston et al., 2011a, 2013a). Figure 3 presents
 319 SEM images (left) and EDX spectra (right) for each particle type detected on stage 3 of the MPS
 320 (particle diameter <0.7 µm), including sea spray, aged sea spray, mineral dust, internally mixed
 321 mineral dust and sea spray, sulfate, smoke, internally mixed mineral dust and smoke, and
 322 organics. Sea spray particles as well as internally mixed mineral dust and sea spray particles

323 were dominant components of the supermicron aerosol loading but are only minor components
324 of submicron aerosol.

325 *Sea Spray*

326 Sea spray particles were characterized by high relative abundance of approximately equal
327 parts Na and Cl, indicating the formation of halite (NaCl). Morphologically, sea spray particles
328 have a cubic shape that represents the crystal structure of halite. Small Mg peaks approximately
329 10% of the height of Na peaks were also observed in NaCl particles and reflect the Na:Mg ratio
330 of seawater. Additional components of sea spray particles include rod-shaped particles
331 containing Ca and S (presumably calcium sulfate) that were often found attached to NaCl
332 particles (Ault et al., 2013; Bondy et al., 2018; Choël et al., 2007). Elements such as N and S that
333 may suggest aging of sea spray were either absent or present in small relative abundance on
334 NaCl components of sea spray particles.

335 *Aged Sea Spray*

336 Aged sea spray was defined by the presence of sea salt components including Na, Mg, K, S,
337 and Cl. In contrast to freshly emitted sea spray particles, aged sea spray has a characteristically
338 low or absent Cl signal with a strong presence of N or S. Figure 3 provides an example of an
339 aged sea spray particle in which Na is high (indicating the presence of salt), but with a low Cl
340 peak (suggesting the particle has been aged). The presence of S in this spectrum may explain the
341 low relative abundance of Cl compared to Na. Sea spray can be aged through reactions with
342 sulfuric acid (H₂SO₄), dinitrogen pentoxide (N₂O₅), and/or nitric acid (HNO₃) which results in Cl
343 depletion and S or N enrichment (Ault et al., 2014; Ault, Guasco, et al., 2013; Behnke et al.,
344 1997; Gaston et al., 2011, 2013; Sobanska et al., 2003). Morphologically, aged sea salt particles

345 had either a similar appearance to fresh sea salt particles, which is often either cubic (as seen in
346 Fig 3), or appeared as a flakey amorphous mass (Hoffman et al., 2004; Laskin et al., 2012; Li et
347 al., 2010).

348 *Mineral Dust*

349 Mineral dust is characterized by the presence of aluminosilicate elements such as Si, Al, Fe,
350 K, Ca, and Mg in EDX spectra, which is consistent with previous studies of African dust
351 (Denjean et al., 2015; Hand et al., 2010; Krueger et al., 2004; Levin et al., 2005; Twohy et al.,
352 2009). Elements such as S and N were not observed in this particle type (Kandler et al., 2018)
353 suggesting that detected dust had not undergone chemical processing during transport. Dust often
354 appeared as a flakey or nodular amorphous mass as exhibited in Fig 3 and previous literature
355 (Krueger et al., 2004; Laskin et al., 2005; Pachauri et al., 2013; Remoundaki et al., 2011).

356 *Internally Mixed Mineral Dust and Sea Spray*

357 Particles containing elements indicative of both mineral dust (Si, Al, Fe, K, Ca, and Mg) and
358 sea salt (approximately equal relative abundances of Na and Cl) were characterized as internally
359 mixed mineral dust and sea spray (Choël et al., 2007; Deboudt et al., 2010; Sobanska et al.,
360 2014). Elements such as S and N were often not present in this particle type, suggesting the
361 particles had not undergone atmospheric aging during transit. Particles containing both dust and
362 sea spray components often appeared as conglomerates of multiple particles with some parts
363 containing more sea spray components and others containing more mineral dust components.

364 *Sulfate*

365 Sulfate-rich particles are a prevalent component of marine submicron aerosol (O'Dowd & de
366 Leeuw, 2007) and characterized here by a dominant S component - often with high relative

367 abundance of C, O, and N. These particles are likely sulfates bound to NH_4^+ such as ammonium
368 sulfate ($(\text{NH}_4)_2\text{SO}_4$) or ammonium bisulfate (NH_4HSO_4) (Hand et al., 2010). The high relative
369 abundance of C indicates a large organic fraction as well. The morphology of sulfate particles
370 appeared smooth and spherical as reported in previous literature (Nájera & Horn, 2009).

371 *Smoke*

372 Smoke particles were identified by the presence of C with K and S likely representing
373 internally mixed organic and black carbon with potassium-containing salts. K is a well-known
374 indicator for biomass burning (Andreae, 1983; Hand et al., 2010; Hudson et al., 2004; J. Li et al.,
375 2003; Murphy et al., 2006; Pósfai et al., 2003), especially in flaming conditions in Savannah fires
376 as opposed to smoldering conditions (Echalar et al., 1995; Maenhaut et al., 1996).
377 Morphologically, smoke particles can be spherical due to aging or coatings but can also appear
378 as aggregates or chains of spheroids (Dang et al., 2021; Hand et al., 2010; Miller et al., 2021;
379 Pósfai et al., 2003). In this study, smoke particles most frequently appeared as small spherical
380 particles.

381 *Internally Mixed Mineral Dust and Smoke*

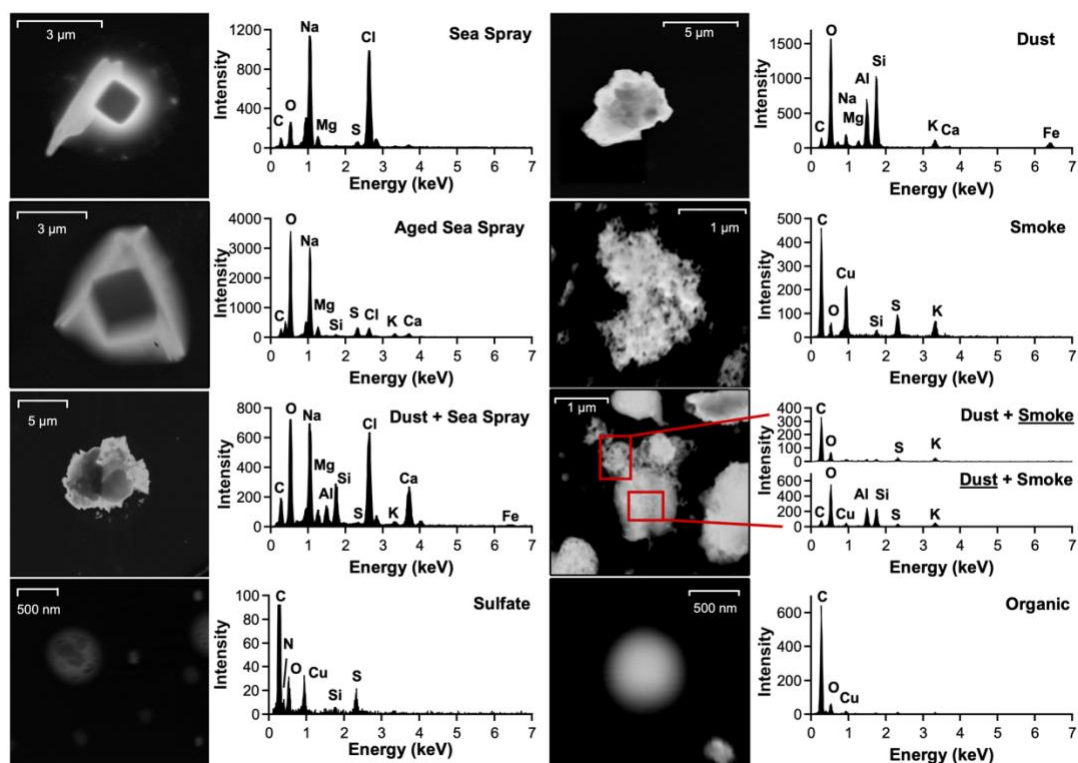
382 Internally mixed mineral dust and smoke particles are characterized by dust components such
383 as Si, Al, Fe, Ca, and Mg with strong contributions of K, S, C, and O. Morphologically, internal
384 mixtures of dust and smoke appear as aggregates of amorphous dust particles with clusters or
385 spheres representing soot from smoke. Single particle chemical analysis of these particles show
386 distinctions between the dust and smoke portion of the particle, with the dust portion having
387 typical dust components (Si, Al, Fe, Ca, and Mg) and the smoke portion having typical smoke
388 components (K and S with C and O). Previous research has observed internal mixing of

389 carbonaceous particles and dust particles in Africa when significant amounts of both biomass
390 burning and dust were present (Hand et al., 2010); however, we show that these internal mixtures
391 can be transported all the way to the Caribbean as well.

392 *Organics*

393 Organic particles are defined by strong signals of C and O with few other elements present, if
394 any (Hand et al., 2010). The absence of S or N, which are often indicative of sulfate and nitrate,
395 respectively, suggests that these particles have undergone minimal chemical aging.

396 Morphologically, organic particles are characterized as small individual spheres. The organics
397 were likely marine in origin (Russell et al., 2010) as they were the smallest particle type
398 observed both during clean marine conditions and during CAT conditions, which indicates they
399 may be a “background” aerosol type (Russell et al., 2010).

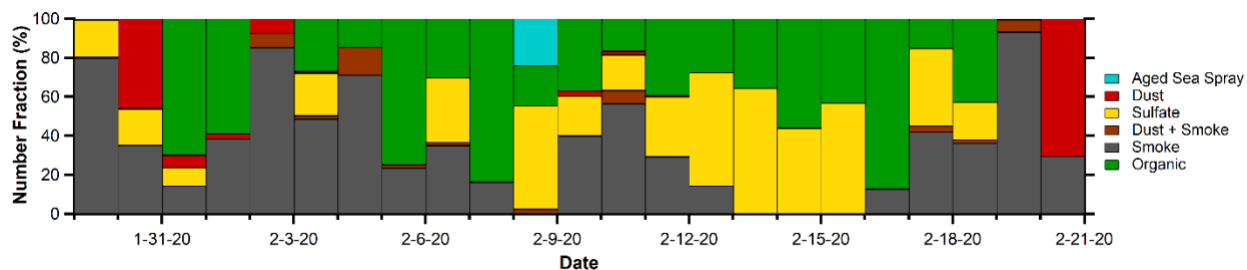


400
 401 **Figure 3:** Characteristic aerosol particle types observed by SEM-EDX images (left) and spectra
 402 (right) in samples collected during the EUREC⁴A/ATOMIC campaign. Spectra for the Dust +
 403 Smoke particle type represent different areas analyzed on the particle with EDX, denoted by the
 404 red boxes.

405
 406 Arrival of Anomalous Wintertime Co-Transported Dust and Smoke

407 Figure 4 presents number fractions for particles detected in the submicron aerosol
 408 throughout the sampling period and reveals a similar trend in smoke particle number fractions to
 409 those of dust mass concentrations in Fig. 2, suggesting that smoke and dust were co-transported
 410 to Barbados from Africa. A similar plot to Fig. 4 that contains temporal chemistry from stage 1
 411 and stage 2 of the MPS (representing supermicron particles >0.7 μm diameter) determined using
 412 CCSEM/EDX analysis can be found in the SI (Figure S2). During the boreal winter, the Sahel

413 region in North Africa experiences its fire season in which large swathes of land are burned and
 414 large plumes of smoke are emitted from the region (Figure S3; Ansmann et al., 2009; Barkley et
 415 al., 2019; Roberts et al., 2009). However, due to the southward shift in the ITCZ during boreal
 416 winter, smoke is expected to be transported primarily to South America (Moran-Zuloaga et al.,
 417 2018; Talbot et al., 1990; Wang et al., 2016). In our study, we observed the arrival of this smoke
 418 on Barbados. These findings are supported by temporal carbon monoxide (CO) column density
 419 measurements that are often used as a tracer for smoke (Figure S4 and S5). Periods that
 420 correspond to clean marine influence are dominated by sulfate and organic particles in the
 421 submicron aerosol (Figure 4). Upon arrival of continental aerosols, wildfire smoke appeared to
 422 dominate the number fraction of submicron aerosol.

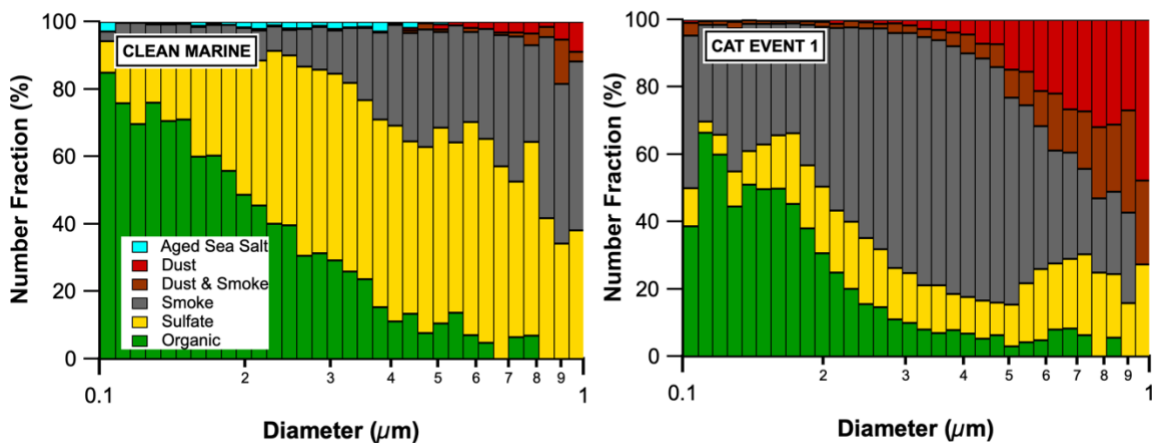


423
 424 **Figure 4:** Temporal evolution of submicron number fractions for different types of aerosol
 425 particles determined by CCSEM/EDX analysis. The total number of particles analyzed for each
 426 day ranges from 1000 to 20,000.

427 Figure 5 presents size-resolved chemical data from CCSEM/EDX analysis from clean
 428 marine periods (average of all clean marine periods) and one exemplary time period influenced
 429 by continental air masses (CAT event 1). Similar plots for other CAT events are provided in the
 430 SI (Figure S6). Average particle diameters for each particle type detected during each sampling
 431 period are also provided in Table S1. Figure 5 shows that in clean marine periods, a small

432 fraction of large particles have both a smoke and a dust signature. This suggests that our “clean
 433 marine conditions” are only “clean” relative to time periods dominated by dust and smoke, rather
 434 than pristine clean marine conditions without any continental aerosol influence. The CAT event
 435 plot in Fig. 5 demonstrates that dust as well as internally mixed dust and smoke particles
 436 dominate in the submicron aerosol loading, followed by smoke. Smoke particles follow as the
 437 next largest particle type. Organics dominate in the smallest size fractions, followed by sulfates,
 438 suggesting a secondary source for sulfate (Bates et al., 1992). Aged sea salt particles were on
 439 average smaller than most dust, internally mixed dust and smoke, and smoke particles. Figure 5
 440 also shows that at a diameter of $\sim 0.1\ \mu\text{m}$ (which is approximately the d_{50} of CCN at S 0.16% in
 441 clean marine conditions and CAT conditions) the composition is dominated by sulfates and
 442 organics in the clean marine conditions, while smoke and organics dominate in the CAT event.
 443 The large decrease in sulfate number fraction during CAT events might be caused by the
 444 condensation of Aitken mode sulfate-containing particles onto larger, long-range transported
 445 particles as indicated in Fig. 2 (Gaston et al., 2010).

446



447

448 **Figure 5:** Number fractions of different types of submicron aerosol particles plotted against

449 particle diameter. The “clean marine” plot (left) includes data from all clean marine sampling
450 periods. The “CAT Event 1” plot (right) includes data from the first period in which dust and
451 wildfire smoke were observed over Barbados (2020/1/29 18:00 – 2020/2/6 6:00 UTC). Particles
452 were organized into 32 size cuts (bins) to maximize resolution of size-resolved chemical data.
453 Particle counts in each bin range from 34 particles to up to 3041 with an average bin count of
454 493 particles for the Clean Marine plot and 973 for the CAT Event plot.

455

456 Changes in Aerosol Hygroscopicity during EUREC⁴A/ATOMIC

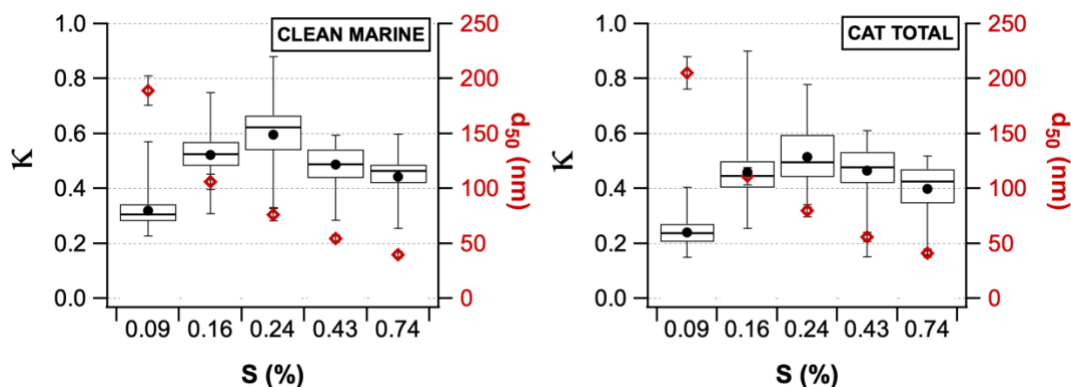
457 Comparisons between κ and submicron single particle elemental composition reveal that
458 smoke particles lower the hygroscopicity of the submicron aerosol compared to marine-derived
459 submicron aerosol in the tropical North Atlantic. Figure 6 presents boxplots for κ values as well
460 as average d_{50} measured at each S during both clean marine conditions and CAT conditions.
461 Both plots show a similar trend in which average κ increases from 0.09% S to 0.24% S. Then,
462 with each subsequent increase in S after 0.24% S, κ decreases as smaller, less hygroscopic
463 particles activate at higher supersaturations. The low hygroscopicity of these smaller particles
464 can be explained by compositional changes in the aerosol loading exhibited in Fig 5, reflecting
465 the shift in particle chemistry from mostly sulfate to mostly organic with decreasing particle size.
466 Also of note is the κ of 0.6 observed for clean marine conditions at 0.24% S, which matches κ
467 measurements for ammonium sulfate particles that can dominate along with sea spray organics
468 during clean marine conditions (Petters & Kreidenweis, 2007).

469 There is also a noticeable drop in average κ between the same supersaturations in clean
470 marine conditions compared to CAT conditions. For example, at 0.16% S, $\kappa=0.52\pm 0.09$ for all
471 clean marine condition periods and $\kappa=0.46\pm 0.10$ for all continental aerosol transport periods.

472 This is likely due to the addition of less hygroscopic material such as dust and smoke particles
473 that are not dominant in clean marine conditions. As expected, trends in average d_{50} for both
474 plots indicate that smaller particles activate as CCN with larger supersaturations. Activation
475 diameters during CAT conditions are also larger than corresponding activation diameters in clean
476 marine conditions for the same supersaturation. This also suggests that the addition of less
477 soluble material from transported smoke particles lowers the hygroscopicity and increases the
478 activation diameter.

479 When comparing hygroscopicity data from this study to previous research, we find both
480 similarities and differences in κ trends. For example, Good et al. (2010) presents data collected in
481 the tropical eastern Atlantic that provides an ideal comparison to our findings. On average, their
482 values for κ in clean marine conditions and during observations of dust transport ($\kappa=1.15-1.4$ and
483 $0.8-0.92$, respectively) were much higher than our observed values. However, Good et al. (2010)
484 shows similarities to our work through the distinct drop in κ between clean marine conditions
485 and CAT conditions which is attributed to the addition of hydrophobic dust to the aerosol
486 loading. Wex et al. (2016) present CCN data from ground-based field sampling in November and
487 April at Ragged Point, Barbados. They show a similar trend in κ in which values increase from
488 0.1% S, peak at 0.2% S, then decrease with each subsequent increase in S. They also found a
489 similar drop in κ upon the arrival of long-range transported aerosols, likely due to less
490 hygroscopic particles from continental sources activating as CCN. A separate study from
491 Kristensen et al. (2016) conducted similar research at Ragged Point, Barbados during the boreal
492 summer. The range in κ values of $0.2-0.5$ match those observed in our work, especially during
493 CAT events. However, Kristensen et al. (2016) determined that concentrations of dust, sea salt,
494 and soot were too small to influence CCN, concluding that sulfates and organics were the

495 primary CCN types. They conclude that the low κ values observed during their sampling were
 496 due to organic compounds activating as CCN. We find similar κ values to Kristensen et al.
 497 (2016) and a similar particle chemistry of the accumulation and Aikten modes during clean
 498 marine conditions, suggesting that organics and sulfates were the primary CCN types during
 499 clean marine conditions studied for the EUREC⁴A and ATOMIC campaigns as well. We also
 500 observe a drop κ from clean marine conditions to CAT events. This drop in κ indicates the
 501 influence of an additional CCN particle type contributed by the CAT events.



502
 503 **Figure 6:** Hygroscopicity parameter κ (left axis, box plots) and corresponding mean
 504 diameter at which 50% of the particles in an aerosol population activate as CCN at a particular S,
 505 also called the critical diameter “d₅₀” (right axis; red markers) for the investigated
 506 supersaturations (S). Whiskers on “d₅₀” markers represent standard deviation values of “d₅₀”.
 507 Black dots in the boxplot indicate κ mean values. Boxes represent the upper quartile, median,
 508 and lower quartile κ values at each S. Whiskers represent the upper and lower limit of κ at each
 509 S.

510

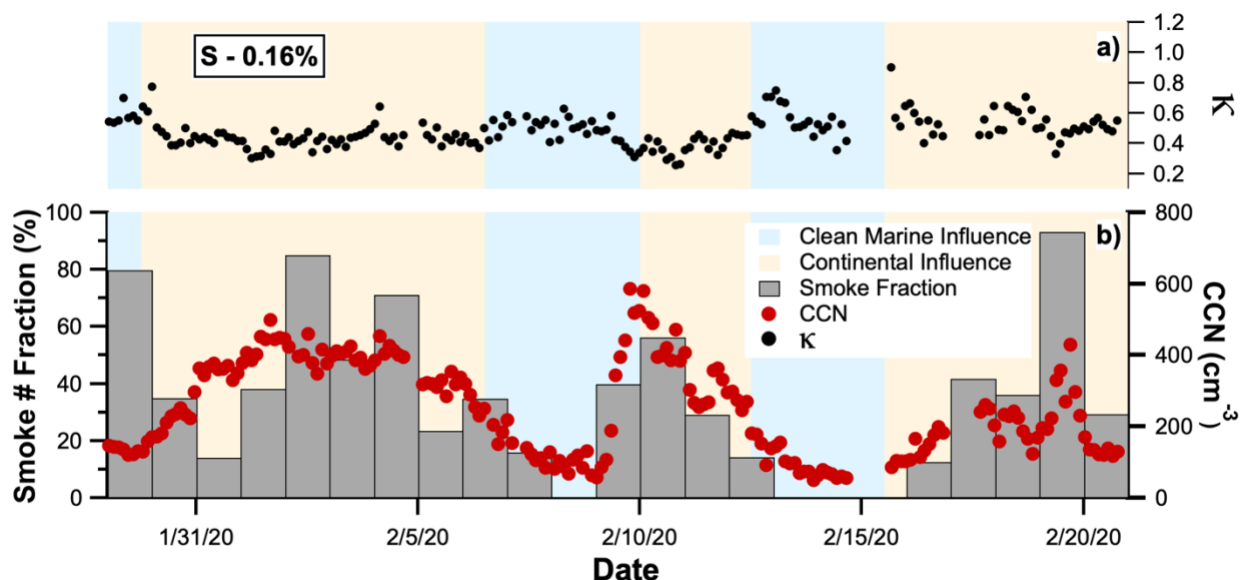
511

512 African Smoke Particles Enhance CCN Concentrations

513 Comparisons between smoke fractions and CCN counts suggest that smoke particles
514 enhance the number of CCN in the tropical North Atlantic MBL. Figure 7 presents two temporal
515 plots of κ (Figure 7a) and smoke number fractions with CCN counts measured at 0.16% S
516 (Figure 7b). Table 1 provides averages of CCN concentrations for each time period shown in
517 Fig. 7b. Table S2 also provides average and median counts of analyzed smoke particles
518 calculated for each CAT event, including CAT Event 3 which had fewer smoke particles and a
519 higher κ compared to other CAT Events. Figure 7 suggests that there is an inverse relationship
520 between κ and smoke number fractions in which an increase in smoke particles results in a
521 decrease in κ . This is likely due to the activation of smoke particles as CCN, which are on
522 average less hygroscopic than the sulfate particles that act as CCN during clean marine
523 conditions. Figure 7b shows a positive correlation between smoke number fractions and CCN
524 counts. A correlation plot of smoke number fraction and CCN concentrations is also provided in
525 Fig. S7 to further emphasize their direct relationship.

526 There are multiple possible explanations for why African smoke particles may have acted
527 as CCN. As shown in Fig. 5, smoke particles are larger than organics and sulfates, on average,
528 and dominate sulfate and organic particle number concentrations upon arrival of long-range
529 transported African aerosols. In this case, the relatively large size of the smoke particles makes
530 for better CCN compared to organics or sulfates via the Kelvin effect (Dusek et al., 2006). The
531 presence of salts in smoke particles has also been shown to be an important component in smoke
532 hygroscopicity and may explain why smoke is efficient as CCN. Previous studies have shown
533 that smoke particles often contain hygroscopic salts such as potassium chloride, potassium
534 sulfate, and potassium nitrate (e.g., KCl, KNO₃, and K₂SO₄) (Dang et al., 2022; Freney et al.,
535 2009; Zauscher et al., 2013). Other research also shows that only small fractions of salts are

536 needed to increase aerosol hygroscopicity (Roberts et al., 2002). Based on CCSEM/EDX
 537 analysis, we find evidence that potassium sulfate salts may be present in transported smoke
 538 particles, and thus may explain the potential for smoke to act as CCN.



539
 540 **Figure 7:** Temporal evolution of hygroscopicity parameter κ (black dots, upper panel) and CCN
 541 number concentration (red dots, lower panel), both measured at $S = 0.16\%$, and smoke particle
 542 number fraction (grey bars, left axis, lower panel). Background color shadings indicate periods
 543 of continental influence (orange) and clean marine influence (blue) determined by HYSPLIT
 544 back trajectories and dust mass concentrations.

545 **Table 1** – Values for average CCN Concentrations and κ measured at 0.16% S during each clean
 546 marine influence period and CAT event sampled during the EUREC⁴A and ATOMIC
 547 campaigns.

Sampling Period	Day/Time	CCN Concentrations (pt/cm^3)	Average κ
Clean Marine Period 1	2020/1/29 0:00 – 2020/1/29 12:00	140 ± 10	0.58 ± 0.07
CAT Event 1	2020/1/29 18:00 – 2020/2/6 6:00	340 ± 90	0.44 ± 0.08
Clean Marine Period 2	2020/2/6 12:00 – 2020/2/9 18:00	150 ± 98	0.50 ± 0.10

CAT Event 2	2020/2/10 0:00 – 2020/2/12 6:00	400 \pm 106	0.38 \pm 0.06
Clean Marine Period 3	2020/2/12 12:00 – 2020/2/15 6:00	100 \pm 42	0.55 \pm 0.10
CAT Event 3	2020/2/15 12:00 – 2020/2/20 – 18:00	190 \pm 75	0.54 \pm 0.10

548

549 **Conclusions**

550 During clean marine conditions, the submicron aerosol loading consists primarily of
551 sulfate and organic particles. CCN measurements determine cloud activation by particles
552 approximately 80 nm in activation diameter with an average $\kappa = 0.52 \pm 0.08$ for 0.16% S.
553 Comparisons between particle size, hygroscopicity, and single particle elemental composition
554 suggest that sulfate particles (likely ammonium sulfate) are the primary CCN particles in clean
555 marine conditions. During the EUREC⁴A/ATOMIC campaign, Barbados received three African
556 aerosol transport events during which we detected mineral dust and smoke particles from
557 northern Africa. Upon the arrival of African aerosols to BACO, CCN average activation
558 diameter increased to approximately 200 nm while the average hygroscopicity of activated
559 particles for all CAT events decreased to $\kappa = 0.45 \pm 0.1$ for 0.16% S. Upon arrival of high
560 concentrations of smoke particles to Barbados, smoke particles dominate the accumulation mode
561 particle loading, decrease aerosol hygroscopicity, and also increase CCN number concentrations,
562 which could also increase the cloud droplet number concentration and alter cloud radiative
563 properties (Twomey, 1974). Overall, we find that smoke has a large effect on CCN number
564 concentrations during the boreal winter when smoke transport is high.

565 The observation of smoke transported to Barbados during the boreal winter also indicates
566 the large geographic extent of African smoke that can impact the MBL. Building upon recent
567 work from Ragged Point and other parts of the tropical and subtropical Atlantic (Holanda et al.,
568 2020; Kacarab et al., 2020; Schill et al., 2020; Zuidema et al., 2018) this work also indicates a

569 need for greater consideration of the impacts of smoke in the MBL, especially during the boreal
570 winter. Previous research conducted at Ragged Point has primarily focused on African dust,
571 which reaches its maximum during the boreal summer when smoke transport is low (Zuidema et
572 al., 2019). To better contextualize our findings, we analysed carbon monoxide column density (a
573 tracer for smoke) as well as aerosol optical depth (AOD; a tracer for dust and smoke) from 2018-
574 2022 (Figure S4 and S5). Figure S4 shows the temporal trends while Fig. S5 show seasonal
575 averages. As expected, AOD peaks in July when dust transport reaches a maximum. However,
576 Fig. S4 and S5 indicate that smoke is decoupled from dust, reaching a maximum in the spring
577 around April and a minimum in the summer when dust transport is highest. This finding suggests
578 that while the dust transport during the EUREC4A/ATOMIC campaigns is higher than average
579 dust loadings during this month (Zuidema et al., 2019), the amount of smoke observed is not
580 unique, but rather characteristic of the region. This is consistent with observations in Amazonia,
581 where smoke and dust transport during boreal winter and spring has been found consistently
582 since the first measurement campaign in 1987 (Talbot et al., 1990; Andreae et al., 2015; Moran-
583 Zuloaga et al., 2018) . Further, wintertime aerosol transport is typically transported at lower
584 altitudes as the height of emission for wintertime aerosols is lower compared to summertime
585 aerosol transport, leading to greater mixing into the MBL (Gutleben et al., 2022; Tsamalis et al.,
586 2013). Thus, smoke may be playing an important role on CCN formation throughout a large
587 portion of the year. This is especially true considering the large size of long-range transported
588 smoke plumes that have a wide geographic extent in which they can affect cloud formation. To
589 conclude, this work highlights the need to characterize African smoke transport to Ragged Point
590 and better understand the role of smoke in cloud formation, radiative forcing, and climate
591 (Pechony & Shindell, 2010; Shindell et al., 2009).

592 **Data Availability**

593 The data will be made publically available in the University of Miami data repository and will be
594 linked with a doi.

595 **Author Contributions**

596 Conceptualization of this work was done by HMR, MLP, OK, and CJG. Collection of samples
597 was conducted by HMR, OK, EB, and PS, while analysis was done by HMR, MLP, OK,>NNL,
598 and ZC. The development of the methods used in this work was done by HMR, MLP, OK, ZC,
599 SC, APA, and CJG. Instrumentation used to conduct this work were provided by MLP, SC,
600 APA, and CJG. Formal analysis of data was performed by HMR, MLP, CP, and OK. Validation
601 of data products was performed by HMR, ZC, SC, APA, and CJG. Computer code used for data
602 analysis was provided by MLP, OK, and APA. Data visualization was performed by HMR,
603 MLP, and OK. PKQ, PZ, CP, and UP helped interpret results. Supervision and project
604 administration duties were done by MLP and CJG. HMR wrote the original draft for publication,
605 and all co-authors reviewed and edited this work.

606 **Competing Interests**

607 Some authors are members of the editorial board of Atmospheric Chemistry and Physics. The
608 peer-review process was guided by an independent editor, and the authors have no other
609 competing interests to declare

610

611 **Acknowledgements**

612 C.J.G. acknowledges an NSF CAREER award (1944958). A portion of this research was
613 performed on project awards (10.46936/lser.proj.2019.50816/60000110 and
614 10.46936/lser.proj.2021.51900/60000361) from the Environmental Molecular Sciences
615 Laboratory, a DOE Office of Science User Facility sponsored by the Biological and
616 Environmental Research program under Contract No. DE-AC05-76RL01830. P.K.Q.
617 acknowledges PMEL contribution number 5353. MLP and CP acknowledge support by the Max
618 Planck Society. P.Z. acknowledges support from the NOAA grant OAR CPO
619 NA19OAR4310379.

620

621

622

623

624

625

626

627

628 References

- 629 Abel, S. J., Haywood, J. M., Highwood, E. J., Li, J., & Buseck, P. R. (2003). Evolution of biomass
630 burning aerosol properties from an agricultural fire in southern Africa. *Geophysical Research*
631 *Letters*, 30(15). <https://doi.org/https://doi.org/10.1029/2003GL017342>
- 632 Adams, A. M., Prospero, J. M., & Zhang, C. (2012). CALIPSO-Derived Three-Dimensional Structure of
633 Aerosol over the Atlantic Basin and Adjacent Continents. *Journal of Climate*, 25, 6862–6879.
- 634 Albrecht, B. A. (1989). Aerosols, cloud microphysics, and fractional cloudiness. *Science*, 245(4923),
635 1227–1230. <https://doi.org/10.1126/science.245.4923.1227>
- 636 Allan, J. D., Baumgardner, D., Raga, G. B., Mayol-Bracero, O. L., Morales-García, F., García-García, F.,
637 Montero-Martínez, G., Borrmann, S., Schneider, J., Mertes, S., Walter, S., Gysel, M., Dusek, U.,
638 Frank, G. P., & Krämer, M. (2008). Clouds and aerosols in Puerto Rico – a new evaluation.
639 *Atmospheric Chemistry and Physics*, 8(5), 1293–1309. <https://doi.org/10.5194/acp-8-1293-2008>
- 640 Andreae, M. O. (1983). Soot Carbon and Excess Fine Potassium: Long-Range Transport of Combustion-
641 Derived Aerosols. *Science*, 220(4602), 1148–1151. <https://doi.org/10.1126/science.220.4602.1148>
- 642 Andreae, M. O. (2019). Emission of trace gases and aerosols from biomass burning -- an updated
643 assessment. *Atmospheric Chemistry and Physics*, 19(13), 8523–8546. [https://doi.org/10.5194/acp-](https://doi.org/10.5194/acp-19-8523-2019)
644 [19-8523-2019](https://doi.org/10.5194/acp-19-8523-2019)
- 645 Ansmann, A., Baars, H., Tesche, M., Müller, D., Althausen, D., Engelmann, R., Pauliquevis, T., &
646 Artaxo, P. (2009). Dust and smoke transport from Africa to South America: Lidar profiling over
647 Cape Verde and the Amazon rainforest. *Geophysical Research Letters*, 36(11).
648 <https://doi.org/https://doi.org/10.1029/2009GL037923>
- 649 Archibald, A. T., Witham, C. S., Ashfold, M. J., Manning, A. J., O’Doherty, S., Grealley, B. R., Young,
650 D., & Shallcross, D. E. (2015). Long-term high frequency measurements of ethane, benzene and
651 methyl chloride at Ragged Point, Barbados: Identification of long-range transport events. *Elementa:*
652 *Science of the Anthropocene*, 3. <https://doi.org/10.12952/journal.elementa.000068>
- 653 Ault, A. P., Guasco, T. L., Baltrusaitis, J., Ryder, O. S., Trueblood, J. v, Collins, D. B., Ruppel, M. J.,
654 Cuadra-Rodriguez, L. A., Prather, K. A., & Grassian, V. H. (2014). Heterogeneous Reactivity of
655 Nitric Acid with Nascent Sea Spray Aerosol: Large Differences Observed between and within
656 Individual Particles. *The Journal of Physical Chemistry Letters*, 5(15), 2493–2500.
657 <https://doi.org/10.1021/jz5008802>
- 658 Ault, A. P., Guasco, T. L., Ryder, O. S., Baltrusaitis, J., Cuadra-Rodriguez, L. A., Collins, D. B., Ruppel,
659 M. J., Bertram, T. H., Prather, K. A., & Grassian, V. H. (2013). Inside versus outside: Ion

660 redistribution in nitric acid reacted sea spray aerosol particles as determined by single particle
661 analysis. *Journal of the American Chemical Society*, 135(39), 14528–14531.
662 <https://doi.org/10.1021/ja407117x>

663 Ault, A. P., Moffet, R. C., Baltrusaitis, J., Collins, D. B., Ruppel, M. J., Cuadra-Rodriguez, L. A., Zhao,
664 D., Guasco, T. L., Ebben, C. J., Geiger, F. M., Bertram, T. H., Prather, K. A., & Grassian, V. H.
665 (2013). Size-Dependent Changes in Sea Spray Aerosol Composition and Properties with Different
666 Seawater Conditions. *Environmental Science & Technology*, 47(11), 5603–5612.
667 <https://doi.org/10.1021/es400416g>

668 Ault, A. P., Peters, T. M., Sawvel, E. J., Casuccio, G. S., Willis, R. D., Norris, G. A., & Grassian, V. H.
669 (2012). Single-Particle SEM-EDX Analysis of Iron-Containing Coarse Particulate Matter in an
670 Urban Environment: Sources and Distribution of Iron within Cleveland, Ohio. *Environmental*
671 *Science & Technology*, 46(8), 4331–4339. <https://doi.org/10.1021/es204006k>

672 Ault, A. P., Zhao, D., Ebben, C. J., Tauber, M. J., Geiger, F. M., Prather, K. A., & Grassian, V. H. (2013).
673 Raman microspectroscopy and vibrational sum frequency generation spectroscopy as probes of the
674 bulk and surface compositions of size-resolved sea spray aerosol particles. *Physical Chemistry*
675 *Chemical Physics*, 15(17), 6206–6214. <https://doi.org/10.1039/C3CP43899F>

676 Barkley, A. E., Olson, N. E., Prospero, J. M., Gatineau, A., Panechou, K., Maynard, N. G., Blackwelder,
677 P., China, S., Ault, A. P., & Gaston, C. J. (2021). Atmospheric Transport of North African Dust-
678 Bearing Supermicron Freshwater Diatoms to South America: Implications for Iron Transport to the
679 Equatorial North Atlantic Ocean. *Geophysical Research Letters*, 48(5), e2020GL090476.
680 <https://doi.org/https://doi.org/10.1029/2020GL090476>

681 Barkley, A. E., Prospero, J. M., Mahowald, N., Hamilton, D. S., Pependorf, K. J., Oehlert, A. M.,
682 Pourmand, A., Gatineau, A., Panechou-Pulcherie, K., Blackwelder, P., & Gaston, C. J. (2019).
683 African biomass burning is a substantial source of phosphorus deposition to the Amazon, Tropical
684 Atlantic Ocean, and Southern Ocean. *Proceedings of the National Academy of Sciences*, 116(33),
685 16216 LP – 16221. <https://doi.org/10.1073/pnas.1906091116>

686 Bates, T. S., Lamb, B. K., Guenther, A., Dignon, J., & Stoiber, R. E. (1992). Sulfur emissions to the
687 atmosphere from natural sources. *Journal of Atmospheric Chemistry*, 14(1), 315–337.
688 <https://doi.org/10.1007/BF00115242>

689 Behnke, W., George, C., Scheer, V., & Zetzsch, C. (1997). Production and decay of ClNO₂ from the
690 reaction of gaseous N₂O₅ with NaCl solution: Bulk and aerosol experiments. *Journal of*
691 *Geophysical Research Atmospheres*, 102(3), 3795–3804. <https://doi.org/10.1029/96jd03057>

692 Behrenfeld, M. J., Moore, R. H., Hostetler, C. A., Graff, J., Gaube, P., Russell, L. M., Chen, G., Doney,
693 S. C., Giovannoni, S., Liu, H., Proctor, C., Bolaños, L. M., Baetge, N., Davie-Martin, C., Westberry,
694 T. K., Bates, T. S., Bell, T. G., Bidle, K. D., Boss, E. S., ... Ziemba, L. (2019). The North Atlantic
695 Aerosol and Marine Ecosystem Study (NAAMES): Science Motive and Mission Overview . In
696 *Frontiers in Marine Science* (Vol. 6). <https://www.frontiersin.org/article/10.3389/fmars.2019.00122>

697 Bondy, A. L., Bonanno, D., Moffet, R. C., Wang, B., Laskin, A., & Ault, A. P. (2018). The diverse
698 chemical mixing state of aerosol particles in the southeastern United States. *Atmospheric Chemistry*
699 *and Physics*, 18(16), 12595–12612. <https://doi.org/10.5194/acp-18-12595-2018>

- 700 Capes, G., Johnson, B., McFiggans, G., Williams, P. ~I., Haywood, J., & Coe, H. (2008). Aging of
701 biomass burning aerosols over West Africa: Aircraft measurements of chemical composition,
702 microphysical properties, and emission ratios. *Journal of Geophysical Research (Atmospheres)*,
703 *113*(D23), D00C15. <https://doi.org/10.1029/2008JD009845>
- 704 Cappa, C. D., Lim, C. Y., Hagan, D. H., Coggon, M., Koss, A., Sekimoto, K., de Gouw, J., Onasch, T. B.,
705 Warneke, C., & Kroll, J. H. (2020). Biomass-burning-derived particles from a wide variety of fuels -
706 - Part 2: Effects of photochemical aging on particle optical and chemical properties. *Atmospheric
707 Chemistry and Physics*, *20*(14), 8511–8532. <https://doi.org/10.5194/acp-20-8511-2020>
- 708 Carlson, T. N., & Prospero, J. M. (1972). The Large-Scale Movement of Saharan Air Outbreaks over the
709 Northern Equatorial Atlantic. *Journal of Applied Meteorology and Climatology*, *11*(2), 283–297.
710 [https://doi.org/10.1175/1520-0450\(1972\)011<0283:TLSMOS>2.0.CO;2](https://doi.org/10.1175/1520-0450(1972)011<0283:TLSMOS>2.0.CO;2)
- 711 Carslaw, K. S., Lee, L. A., Reddington, C. L., Pringle, K. J., Rap, A., Forster, P. M., Mann, G. W.,
712 Spracklen, D. v, Woodhouse, M. T., Regayre, L. A., & Pierce, J. R. (2013). Large contribution of
713 natural aerosols to uncertainty in indirect forcing. *Nature*, *503*(7474), 67–71.
714 <https://doi.org/10.1038/nature12674>
- 715 Chin, M., Diehl, T., Tan, Q., Prospero, J. M., Kahn, R. A., Remer, L. A., Yu, H., Sayer, A. M., Bian, H.,
716 Geogdzhayev, I. v, Holben, B. N., Howell, S. G., Huebert, B. J., Hsu, N. C., Kim, D., Kucsera, T.
717 L., Levy, R. C., Mishchenko, M. I., Pan, X., ... Zhao, X.-P. (2014). Multi-decadal aerosol variations
718 from 1980 to 2009: a perspective from observations and a global model. *Atmospheric Chemistry and
719 Physics*, *14*(7), 3657–3690. <https://doi.org/10.5194/acp-14-3657-2014>
- 720 Choël, M., Deboudt, K., Flament, P., Aimo, L., & Mériaux, X. (2007). Single-particle analysis of
721 atmospheric aerosols at Cape Gris-Nez, English Channel: Influence of steel works on iron
722 apportionment. *Atmospheric Environment*, *41*(13), 2820–2830.
723 <https://doi.org/https://doi.org/10.1016/j.atmosenv.2006.11.038>
- 724 Dang, C., Segal-Rozenhaimer, M., Che, H., Zhang, L., Formenti, P., Taylor, J., Dobracki, A., Purdue, S.,
725 Wong, P.-S., Nenes, A., Sedlacek, A., Coe, H., Redemann, J., Zuidema, P., & Haywood, J. (2021).
726 Biomass burning and marine aerosol processing over the southeast Atlantic Ocean: A TEM single
727 particle analysis. *Atmos. Chem. Phys. Discuss.*, *2021*, 1–30. <https://doi.org/10.5194/acp-2021-724>
- 728 Dang, C., Segal-Rozenhaimer, M., Che, H., Zhang, L., Formenti, P., Taylor, J., Dobracki, A., Purdue, S.,
729 Wong, P.-S., Nenes, A., Sedlacek III, A., Coe, H., Redemann, J., Zuidema, P., Howell, S., &
730 Haywood, J. (2022). Biomass burning and marine aerosol processing over the southeast Atlantic
731 Ocean: a TEM single-particle analysis. *Atmospheric Chemistry and Physics*, *22*(14), 9389–9412.
732 <https://doi.org/10.5194/acp-22-9389-2022>
- 733 Deboudt, K., Flament, P., Choël, M., Gloter, A., Sobanska, S., & Colliex, C. (2010). Mixing state of
734 aerosols and direct observation of carbonaceous and marine coatings on African dust by individual
735 particle analysis. *Journal of Geophysical Research: Atmospheres*, *115*(D24).
736 <https://doi.org/https://doi.org/10.1029/2010JD013921>
- 737 Denjean, C., Caquineau, S., Desboeufs, K., Laurent, B., Maille, M., Quiñones Rosado, M., Vallejo, P.,
738 Mayol-Bracero, O. L., & Formenti, P. (2015). Long-range transport across the Atlantic in
739 summertime does not enhance the hygroscopicity of African mineral dust. *Geophysical Research
740 Letters*, *42*(18), 7835–7843. <https://doi.org/https://doi.org/10.1002/2015GL065693>

- 741 Dusek, U., Frank, G. P., Hildebrandt, L., Curtius, J., Schneider, J., Walter, S., Chand, D., Drewnick, F.,
742 Hings, S., Jung, D., Borrmann, S., & Andreae, M. O. (2006). Size Matters More Than Chemistry for
743 Cloud-Nucleating Ability of Aerosol Particles. *Science*, *312*(5778), 1375–1378.
744 <https://doi.org/10.1126/science.1125261>
- 745 Echalar, F., Gaudichet, A., Cachier, H., & Artaxo, P. (1995). Aerosol emissions by tropical forest and
746 savanna biomass burning: Characteristic trace elements and fluxes. *Geophysical Research Letters*,
747 *22*(22), 3039–3042. <https://doi.org/10.1029/95GL03170>
- 748 Edwards, E.-L., Corral, A. F., Dadashazar, H., Barkley, A. E., Gaston, C. J., Zuidema, P., & Sorooshian,
749 A. (2021). Impact of various air mass types on cloud condensation nuclei concentrations along
750 coastal southeast Florida. *Atmospheric Environment*, *254*, 118371.
751 <https://doi.org/10.1016/j.atmosenv.2021.118371>
- 752 Forster, P., Storelvmo, T., Armour, K., William, C., Dufresne, J.-L., Frame, D., Lunt, D., Mauritsen, T.,
753 Palmer, M., Watanabe, M., Wild, M., & Zhang, H. (2021). Chapter 7: The Earth’s energy budget,
754 climate feedbacks, and climate sensitivity. *Climate Change 2021: The Physical Science Basis*,
755 *Contributi*.
- 756 Freney, E. J., Martin, S. T., & Buseck, P. R. (2009). Deliquescence and efflorescence of potassium salts
757 relevant to biomass-burning aerosol particles. *Aerosol Science and Technology*, *43*(8), 799–807.
758 <https://doi.org/10.1080/02786820902946620>
- 759 Gaston, C. J., Furutani, H., Guazzotti, S. A., Coffee, K. R., Bates, T. S., Quinn, P. K., Aluwihare, L. I.,
760 Mitchell, B. G., & Prather, K. A. (2011). Unique ocean-derived particles serve as a proxy for
761 changes in ocean chemistry. *Journal of Geophysical Research Atmospheres*, *116*(18), 1–13.
762 <https://doi.org/10.1029/2010JD015289>
- 763 Gaston, C. J., Pratt, K. A., Qin, X., & Prather, K. A. (2010). Real-time detection and mixing state of
764 methanesulfonate in single particles at an inland urban location during a phytoplankton bloom.
765 *Environmental Science and Technology*, *44*(5), 1566–1572. <https://doi.org/10.1021/es902069d>
- 766 Gaston, C. J., Quinn, P. K., Bates, T. S., Gilman, J. B., Bon, D. M., Kuster, W. C., & Prather, K. A.
767 (2013). The impact of shipping, agricultural, and urban emissions on single particle chemistry
768 observed aboard the R/V Atlantis during CalNex. *Journal of Geophysical Research Atmospheres*,
769 *118*(10), 5003–5017. <https://doi.org/10.1002/jgrd.50427>
- 770 Giordano, M., Espinoza, C., & Asa-Awuku, A. (2015). Experimentally measured morphology of biomass
771 burning aerosol and its impacts on CCN ability. *Atmospheric Chemistry and Physics*, *15*(4), 1807–
772 1821. <https://doi.org/10.5194/acp-15-1807-2015>
- 773 Good, N., Topping, D. O., Allan, J. D., Flynn, M., Fuentes, E., Irwin, M., Williams, P. I., Coe, H., &
774 McFiggans, G. (2010). Consistency between parameterisations of aerosol hygroscopicity and CCN
775 activity during the RHaMBLe discovery cruise. *Atmos. Chem. Phys.*, *10*(7), 3189–3203.
776 <https://doi.org/10.5194/acp-10-3189-2010>
- 777 Gutleben, M., Groß, S., Heske, C., & Wirth, M. (2022). Wintertime Saharan dust transport towards the
778 Caribbean: an airborne lidar case study during EUREC⁴S. *Atmospheric Chemistry and Physics*,
779 *22*(11), 7319–7330. <https://doi.org/10.5194/acp-22-7319-2022>
- 780 Hand, V. L., Capes, G., Vaughan, D. J., Formenti, P., Haywood, J. M., & Coe, H. (2010). Evidence of
781 internal mixing of African dust and biomass burning particles by individual particle analysis using

782 electron beam techniques. *Journal of Geophysical Research: Atmospheres*, 115(D13).
783 <https://doi.org/https://doi.org/10.1029/2009JD012938>

784 Hennigan, C. J., Miracolo, M. A., Engelhart, G. J., May, A. A., Presto, A. A., Lee, T., Sullivan, A. P.,
785 McMeeking, G. R., Coe, H., Wold, C. E., Hao, W.-M., Gilman, J. B., Kuster, W. C., de Gouw, J.,
786 Schichtel, B. A., Collett Jr., J. L., Kreidenweis, S. M., & Robinson, A. L. (2011). Chemical and
787 physical transformations of organic aerosol from the photo-oxidation of open biomass burning
788 emissions in an environmental chamber. *Atmospheric Chemistry and Physics*, 11(15), 7669–7686.
789 <https://doi.org/10.5194/acp-11-7669-2011>

790 Hennigan, C. J., Sullivan, A. P., Collett Jr., J. L., & Robinson, A. L. (2010). Levoglucosan stability in
791 biomass burning particles exposed to hydroxyl radicals. *Geophysical Research Letters*, 37(9).
792 <https://doi.org/https://doi.org/10.1029/2010GL043088>

793 Hodshire, A. L., Akherati, A., Alvarado, M. J., Brown-Steiner, B., Jathar, S. H., Jimenez, J. L.,
794 Kreidenweis, S. M., Lonsdale, C. R., Onasch, T. B., Ortega, A. M., & Pierce, J. R. (2019). Aging
795 Effects on Biomass Burning Aerosol Mass and Composition: A Critical Review of Field and
796 Laboratory Studies. *Environmental Science & Technology*, 53(17), 10007–10022.
797 <https://doi.org/10.1021/acs.est.9b02588>

798 Hoffman, R. C., Laskin, A., & Finlayson-Pitts, B. J. (2004). Sodium nitrate particles: physical and
799 chemical properties during hydration and dehydration, and implications for aged sea salt aerosols.
800 *Journal of Aerosol Science*, 35(7), 869–887.
801 <https://doi.org/https://doi.org/10.1016/j.jaerosci.2004.02.003>

802 Holanda, B. A., Pöhlker, M. L., Walter, D., Saturno, J., Sörgel, M., Ditas, J., Ditas, F., Schulz, C., Franco,
803 M. A., Wang, Q., Donth, T., Artaxo, P., Barbosa, H. M. J., Borrmann, S., Braga, R., Brito, J.,
804 Cheng, Y., Dollner, M., Kaiser, J. W., ... Pöhlker, C. (2020). Influx of African biomass burning
805 aerosol during the Amazonian dry season through layered transatlantic transport of black carbon-
806 rich smoke. *Atmospheric Chemistry and Physics*, 20(8), 4757–4785. <https://doi.org/10.5194/acp-20-4757-2020>

807

808 Hoppel, W. A., Frick, G. M., & Larson, R. E. (1986). Effect of nonprecipitating clouds on the aerosol size
809 distribution in the marine boundary layer. *Geophysical Research Letters*, 13(2), 125–128.
810 <https://doi.org/https://doi.org/10.1029/GL013i002p00125>

811 Hudson, P. K., Murphy, D. M., Cziczo, D. J., Thomson, D. S., de Gouw, J. A., Warneke, C., Holloway, J.,
812 Jost, H.-J., & Hübler, G. (2004). Biomass-burning particle measurements: Characteristic
813 composition and chemical processing. *Journal of Geophysical Research: Atmospheres*, 109(D23).
814 <https://doi.org/https://doi.org/10.1029/2003JD004398>

815 Kacarab, M., Thornhill, K. L., Dobracki, A., Howell, S. G., O'Brien, J. R., Freitag, S., Poellot, M. R.,
816 Wood, R., Zuidema, P., Redemann, J., & Nenes, A. (2020). Biomass burning aerosol as a modulator
817 of the droplet number in the southeast Atlantic region. *Atmos. Chem. Phys.*, 20(5), 3029–3040.
818 <https://doi.org/10.5194/acp-20-3029-2020>

819 Kitto, M. E., & Anderson, D. L. (1988). The use of Whatman-41 filters for particle. *Atmospheric*
820 *Environment* (1967), 22(11), 2629–2630. [https://doi.org/https://doi.org/10.1016/0004-](https://doi.org/https://doi.org/10.1016/0004-6981(88)90500-8)
821 [6981\(88\)90500-8](https://doi.org/https://doi.org/10.1016/0004-6981(88)90500-8)

- 822 Klingebiel, M., Ghate, V. P., Naumann, A. K., Ditas, F., Pöhlker, M. L., Pöhlker, C., Kandler, K.,
823 Konow, H., & Stevens, B. (2019). Remote Sensing of Sea Salt Aerosol below Trade Wind Clouds.
824 *Journal of the Atmospheric Sciences*, 76(5), 1189–1202. <https://doi.org/10.1175/JAS-D-18-0139.1>
- 825 Kononov, I. B., Golovushkin, N. A., Beekmann, M., & Andreae, M. O. (2021). Insights into the aging
826 of biomass burning aerosol from satellite observations and 3D atmospheric modeling: evolution of
827 the aerosol optical properties in Siberian wildfire plumes. *Atmospheric Chemistry and Physics*,
828 21(1), 357–392. <https://doi.org/10.5194/acp-21-357-2021>
- 829 Kristensen, T. B., Müller, T., Kandler, K., Benker, N., Hartmann, M., Prospero, J. M., Wiedensohler, A.,
830 & Stratmann, F. (2016). Properties of cloud condensation nuclei (CCN) in the trade wind marine
831 boundary layer of the western North Atlantic. *Atmos. Chem. Phys.*, 16(4), 2675–2688.
832 <https://doi.org/10.5194/acp-16-2675-2016>
- 833 Krueger, B. J., Grassian, V. H., Cowin, J. P., & Laskin, A. (2004). Heterogeneous chemistry of individual
834 mineral dust particles from different dust source regions: the importance of particle mineralogy.
835 *Atmospheric Environment*, 38(36), 6253–6261.
836 <https://doi.org/https://doi.org/10.1016/j.atmosenv.2004.07.010>
- 837 Laskin, A., Moffet, R. C., Gilles, M. K., Fast, J. D., Zaveri, R. A., Wang, B., Nigge, P., & Shutthanandan,
838 J. (2012). Tropospheric chemistry of internally mixed sea salt and organic particles: Surprising
839 reactivity of NaCl with weak organic acids. *Journal of Geophysical Research: Atmospheres*,
840 117(D15). <https://doi.org/https://doi.org/10.1029/2012JD017743>
- 841 Laskin, A., Wietsma, T. W., Krueger, B. J., & Grassian, V. H. (2005). Heterogeneous chemistry of
842 individual mineral dust particles with nitric acid: A combined CCSEM/EDX, ESEM, and ICP-MS
843 study. *Journal of Geophysical Research: Atmospheres*, 110(D10).
844 <https://doi.org/https://doi.org/10.1029/2004JD005206>
- 845 Latham, T. L., Beyersdorf, A. J., Thornhill, K. L., Winstead, E. L., Cubison, M. J., Hecobian, A.,
846 Jimenez, J. L., Weber, R. J., Anderson, B. E., & Nenes, A. (2013). Analysis of CCN activity of
847 Arctic aerosol and Canadian biomass burning during summer 2008. *Atmospheric Chemistry and
848 Physics*, 13(5), 2735–2756. <https://doi.org/10.5194/acp-13-2735-2013>
- 849 Levin, Z., Teller, A., Ganor, E., & Yin, Y. (2005). On the interactions of mineral dust, sea-salt particles,
850 and clouds: A measurement and modeling study from the Mediterranean Israeli Dust Experiment
851 campaign. *Journal of Geophysical Research: Atmospheres*, 110(D20).
852 <https://doi.org/https://doi.org/10.1029/2005JD005810>
- 853 Li, J., Pósfai, M., Hobbs, P. v., & Buseck, P. R. (2003). Individual aerosol particles from biomass burning
854 in southern Africa: 2, Compositions and aging of inorganic particles. *Journal of Geophysical
855 Research: Atmospheres*, 108(D13). <https://doi.org/https://doi.org/10.1029/2002JD002310>
- 856 Li, W., Shao, L., Wang, Z., Shen, R., Yang, S., & Tang, U. (2010). Size, composition, and mixing state of
857 individual aerosol particles in a South China coastal city. *Journal of Environmental Sciences*, 22(4),
858 561–569. [https://doi.org/https://doi.org/10.1016/S1001-0742\(09\)60146-7](https://doi.org/https://doi.org/10.1016/S1001-0742(09)60146-7)
- 859 Maenhaut, W., Salma, I., Cafmeyer, J., Annegarn, H. J., & Andreae, M. O. (1996). Regional atmospheric
860 aerosol composition and sources in the eastern Transvaal, South Africa, and impact of biomass
861 burning. *Journal of Geophysical Research: Atmospheres*, 101(D19), 23631–23650.
862 <https://doi.org/https://doi.org/10.1029/95JD02930>

- 863 McCoy, D. T., Burrows, S. M., Wood, R., Grosvenor, D. P., Elliott, S. M., Ma, P.-L., Rasch, P. J., &
864 Hartment, D. L. (2022). Natural aerosols explain seasonal and spatial patterns of Southern Ocean
865 cloud albedo. *Science Advances*, *1*(6), e1500157. <https://doi.org/10.1126/sciadv.1500157>
- 866 McFiggans, G., Artaxo, P., Baltensperger, U., Coe, H., Facchini, M. C., Feingold, G., Fuzzi, S., Gysel,
867 M., Laaksonen, A., Lohmann, U., Mentel, T. F., Murphy, D. M., O'Dowd, C. D., Snider, J. R., &
868 Weingartner, E. (2006). The effect of physical and chemical aerosol properties on warm cloud
869 droplet activation. *Atmospheric Chemistry and Physics*, *6*(9), 2593–2649.
870 <https://doi.org/10.5194/acp-6-2593-2006>
- 871 Miles, J. C., Crutzen, P. J., & Goldammer, J. G. (1995). Fire in the Environment: The Ecological,
872 Atmospheric and Climatic Importance of Vegetation Fires. *Journal of Ecology*, *83*, 549.
- 873 Miller, R. M., McFarquhar, G. M., Rauber, R. M., O'Brien, J. R., Gupta, S., Segal-Rozenhaimer, M.,
874 Dobracki, A. N., Sedlacek, A. J., Burton, S. P., Howell, S. G., Freitag, S., & Dang, C. (2021).
875 Observations of supermicron-sized aerosols originating from biomass burning in southern Central
876 Africa. *Atmos. Chem. Phys.*, *21*(19), 14815–14831. <https://doi.org/10.5194/acp-21-14815-2021>
- 877 Moran-Zuloaga, D., Ditas, F., Walter, D., Saturno, J., Brito, J., Carbone, S., Chi, X., de Angelis, I., Baars,
878 H., Godoi, R. H. M., Heese, B., Holanda, B. A., Lavrič, J. v, Martin, S. T., Ming, J., Pöhlker, M. L.,
879 Ruckteschler, N., Su, H., Wang, Y., ... Pöhlker, C. (2018). Long-term study on coarse mode
880 aerosols in the Amazon rain forest with the frequent intrusion of Saharan dust plumes. *Atmospheric
881 Chemistry and Physics*, *18*(13), 10055–10088. <https://doi.org/10.5194/acp-18-10055-2018>
- 882 Murphy, D. M., Cziczo, D. J., Froyd, K. D., Hudson, P. K., Matthew, B. M., Middlebrook, A. M., Peltier,
883 R. E., Sullivan, A., Thomson, D. S., & Weber, R. J. (2006). Single-particle mass spectrometry of
884 tropospheric aerosol particles. *Journal of Geophysical Research: Atmospheres*, *111*(D23).
885 <https://doi.org/https://doi.org/10.1029/2006JD007340>
- 886 Nájera, J. J., & Horn, A. B. (2009). Infrared spectroscopic study of the effect of oleic acid on the
887 deliquescence behaviour of ammonium sulfate aerosol particles. *Physical Chemistry Chemical
888 Physics*, *11*(3), 483–494. <https://doi.org/10.1039/B812182F>
- 889 O'Dowd, C. D., & de Leeuw, G. (2007). Marine aerosol production: a review of the current knowledge.
890 *Philosophical Transactions of the Royal Society A: Mathematical, Physical and Engineering
891 Sciences*, *365*(1856), 1753–1774. <https://doi.org/10.1098/rsta.2007.2043>
- 892 O'Dowd, C. D., Facchini, M. C., Cavalli, F., Ceburnis, D., Mircea, M., Decesari, S., Fuzzi, S., Yoon, Y.
893 J., & Putaud, J.-P. (2004). Biogenically driven organic contribution to marine aerosol. *Nature*,
894 *431*(7009), 676–680. <https://doi.org/10.1038/nature02959>
- 895 Pachauri, T., Singla, V., Satsangi, A., Lakhani Anita, & Kumari, K. M. (2013). SEM-EDX
896 Characterization of Individual Coarse Particles in Agra, India. *Aerosol and Air Quality Research*,
897 *13*(2), 523–536. <https://doi.org/10.4209/aaqr.2012.04.0095>
- 898 Petters, M. D., & Kreidenweis, S. M. (2007). A single parameter representation of hygroscopic growth
899 and cloud condensation nucleus activity. *Atmospheric Chemistry and Physics*, *7*(8), 1961–1971.
900 <https://doi.org/10.5194/acp-7-1961-2007>
- 901 Pierce, J. R., Chen, K., & Adams, P. J. (2007). Contribution of primary carbonaceous aerosol to cloud
902 condensation nuclei: processes and uncertainties evaluated with a global aerosol microphysics

903 model. *Atmospheric Chemistry and Physics*, 7(20), 5447–5466. [https://doi.org/10.5194/acp-7-5447-](https://doi.org/10.5194/acp-7-5447-2007)
904 2007

905 Pósfai, M., Simonics, R., Li, J., Hobbs, P. v., & Buseck, P. R. (2003). Individual aerosol particles from
906 biomass burning in southern Africa: 1. Compositions and size distributions of carbonaceous
907 particles. *Journal of Geophysical Research: Atmospheres*, 108(D13).
908 <https://doi.org/https://doi.org/10.1029/2002JD002291>

909 Prospero, J. M. (1968). atmospheric dust studies on Barbados. *Bulletin of the American Meteorological*
910 *Society*, 49(6), 645–652. <https://doi.org/10.1175/1520-0477-49.6.645>

911 Prospero, J. M. (1999). Long-range transport of mineral dust in the global atmosphere: Impact of African
912 dust on the environment of the southeastern United States. *Proceedings of the National Academy of*
913 *Sciences*, 96(7), 3396 LP – 3403. <https://doi.org/10.1073/pnas.96.7.3396>

914 Prospero, J. M., Barkley, A. E., Gaston, C. J., Gatineau, A., Campos y Sansano, A., & Panechou, K.
915 (2020). Characterizing and Quantifying African Dust Transport and Deposition to South America:
916 Implications for the Phosphorus Budget in the Amazon Basin. *Global Biogeochemical Cycles*,
917 34(9), e2020GB006536. <https://doi.org/https://doi.org/10.1029/2020GB006536>

918 Prospero, J. M., Blades, E., Mathison, G., & Naidu, R. (2005). Interhemispheric transport of viable fungi
919 and bacteria from Africa to the Caribbean with soil dust. *Aerobiologia*, 21(1), 1–19.
920 <https://doi.org/10.1007/s10453-004-5872-7>

921 Prospero, J. M., Collard, F.-X., Molinié, J., & Jeannot, A. (2014). Characterizing the annual cycle of
922 African dust transport to the Caribbean Basin and South America and its impact on the environment
923 and air quality. *Global Biogeochemical Cycles*, 28(7), 757–773.
924 <https://doi.org/https://doi.org/10.1002/2013GB004802>

925 Prospero, J. M., Delany, A. C., Delany, A. C., & Carlson, T. N. (2021). The Discovery of African Dust
926 Transport to the Western Hemisphere and the Saharan Air Layer: A History. *Bulletin of the*
927 *American Meteorological Society*, 102(6), E1239–E1260. [https://doi.org/10.1175/BAMS-D-19-](https://doi.org/10.1175/BAMS-D-19-0309.1)
928 0309.1

929 Prospero, J. M., Glaccum, R. A., & Nees, R. T. (1981). Atmospheric transport of soil dust from Africa to
930 South America. *Nature*, 289(5798), 570–572. <https://doi.org/10.1038/289570a0>

931 Prospero, J. M., & Lamb, P. J. (n.d.). *prospero2003*.

932 Prospero, J. M., & Lamb, P. J. (2003). African Droughts and Dust Transport to the Caribbean: Climate
933 Change Implications. *Science*, 302(5647), 1024–1027. <https://doi.org/10.1126/science.1089915>

934 Prospero, J. M., & Mayol-Bracero, O. L. (2013). Understanding the Transport and Impact of African Dust
935 on the Caribbean Basin. *Bulletin of the American Meteorological Society*, 94(9), 1329–1337.
936 <https://doi.org/10.1175/BAMS-D-12-00142.1>

937 Pszenny, A., Fischer, C., Mendez, A., & Zetwo, M. (1993). Direct comparison of cellulose and quartz
938 fiber filters for sampling submicrometer aerosols in the marine boundary layer. *Atmospheric*
939 *Environment. Part A. General Topics*, 27(2), 281–284. [https://doi.org/https://doi.org/10.1016/0960-](https://doi.org/https://doi.org/10.1016/0960-1686(93)90359-7)
940 1686(93)90359-7

- 941 Quinn, P. K., Bates, T. S., Coffman, D. J., & Covert, D. S. (2008). Influence of particle size and
 942 chemistry on the cloud nucleating properties of aerosols. *Atmospheric Chemistry and Physics*, 8(4),
 943 1029–1042. <https://doi.org/10.5194/acp-8-1029-2008>
- 944 Quinn, P. K., Thompson, E. J., Coffman, D. J., Baidar, S., Bariteau, L., Bates, T. S., Bigorre, S., Brewer,
 945 A., de Boer, G., de Szoeki, S. P., Drushka, K., Foltz, G. R., Intrieri, J., Iyer, S., Fairall, C. W.,
 946 Gaston, C. J., Jansen, F., Johnson, J. E., Krüger, O. O., ... Zuidema, P. (2021). Measurements from
 947 the RV Ronald H. Brown and related platforms as part of the Atlantic Tradewind Ocean-
 948 Atmosphere Mesoscale Interaction Campaign (ATOMIC). *Earth Syst. Sci. Data*, 13(4), 1759–1790.
 949 <https://doi.org/10.5194/essd-13-1759-2021>
- 950 Rauber, R. M., Stevens, B., Ochs, H. T., Knight, C., Albrecht, B. A., Blyth, A. M., Fairall, C. W., Jensen,
 951 J. B., Lasher-Trapp, S. G., Mayol-Bracero, O. L., Vali, G., Anderson, J. R., Baker, B. A., Bandy, A.
 952 R., Burnet, E., Brenguier, J.-L., Brewer, W. A., Brown, P. R. A., Chuang, R., ... Zuidema, P.
 953 (2007). Rain in Shallow Cumulus Over the Ocean: The RICO Campaign. *Bulletin of the American*
 954 *Meteorological Society*, 88(12), 1912–1928. <https://doi.org/10.1175/BAMS-88-12-1912>
- 955 Reid, J. S., Hobbs, P. v., Ferek, R. J., Blake, D. R., Martins, J. V., Dunlap, M. R., & Liousse, C. (1998).
 956 Physical, chemical, and optical properties of regional hazes dominated by smoke in Brazil. *Journal*
 957 *of Geophysical Research: Atmospheres*, 103(D24), 32059–32080.
 958 <https://doi.org/https://doi.org/10.1029/98JD00458>
- 959 Reid, J. S., Koppmann, R., Eck, T. F., & Eleuterio, D. P. (2005). A review of biomass burning emissions
 960 part II: intensive physical properties of biomass burning particles. *Atmospheric Chemistry and*
 961 *Physics*, 5(3), 799–825. <https://doi.org/10.5194/acp-5-799-2005>
- 962 Remoundaki, E., Bourliva, A., Kokkalis, P., Mamouri, R. E., Papayannis, A., Grigoratos, T., Samara, C.,
 963 & Tsezos, M. (2011). PM10 composition during an intense Saharan dust transport event over Athens
 964 (Greece). *Science of The Total Environment*, 409(20), 4361–4372.
 965 <https://doi.org/https://doi.org/10.1016/j.scitotenv.2011.06.026>
- 966 Roberts, G. C., Artaxo, P., Zhou, J., Swietlicki, E., & Andreae, M. O. (2002). Sensitivity of CCN spectra
 967 on chemical and physical properties of aerosol: A case study from the Amazon Basin. *Journal of*
 968 *Geophysical Research: Atmospheres*, 107(D20), LBA 37-1-LBA 37-18.
 969 <https://doi.org/https://doi.org/10.1029/2001JD000583>
- 970 Roberts, G. C., & Nenes, A. (2005). A Continuous-Flow Streamwise Thermal-Gradient CCN Chamber
 971 for Atmospheric Measurements. *Aerosol Science and Technology*, 39(3), 206–221.
 972 <https://doi.org/10.1080/027868290913988>
- 973 Roberts, G., Wooster, M. J., & Lagoudakis, E. (2009). Annual and diurnal african biomass burning
 974 temporal dynamics. *Biogeosciences*, 6(5), 849–866. <https://doi.org/10.5194/bg-6-849-2009>
- 975 Rogers, C. F., Hudson, J. G., Zielinska, B., Tanner, R. L., Hallett, J., & Watson, J. G. (1991). *Cloud*
 976 *condensation nuclei from biomass burning*. Massachusetts Inst of Tech Press.
 977 http://inis.iaea.org/search/search.aspx?orig_q=RN:23066783
- 978 Rolph, G., Stein, A., & Stunder, B. (2017). Real-time Environmental Applications and Display sYstem:
 979 READY. *Environmental Modelling & Software*, 95, 210–228.
 980 <https://doi.org/https://doi.org/10.1016/j.envsoft.2017.06.025>

- 981 Rose, D., Gunthe, S. S., Mikhailov, E., Frank, G. P., Dusek, U., Andreae, M. O., & Pöschl, U. (2008).
 982 Calibration and measurement uncertainties of a continuous-flow cloud condensation nuclei counter
 983 (DMT-CCNC): CCN activation of ammonium sulfate and sodium chloride aerosol particles in
 984 theory and experiment. *Atmospheric Chemistry and Physics*, 8(5), 1153–1179.
 985 <https://doi.org/10.5194/acp-8-1153-2008>
- 986 Rosenfeld, D., Rudich, Y., & Lahav, R. (2001). Desert dust suppressing precipitation: A possible
 987 desertification feedback loop. *Proceedings of the National Academy of Sciences*, 98(11), 5975 LP –
 988 5980. <https://doi.org/10.1073/pnas.101122798>
- 989 Russell, L. M., Hawkins, L. N., Frossard, A. A., Quinn, P. K., & Bates, T. S. (2010). Carbohydrate-like
 990 composition of submicron atmospheric particles and their production from ocean bubble bursting.
 991 *Proceedings of the National Academy of Sciences*, 107(15), 6652 LP – 6657.
 992 <https://doi.org/10.1073/pnas.0908905107>
- 993 Savoie, D. L., Arimoto, R., Keene, W. C., Prospero, J. M., Duce, R. A., & Galloway, J. N. (2002). Marine
 994 biogenic and anthropogenic contributions to non-sea-salt sulfate in the marine boundary layer over
 995 the North Atlantic Ocean. *Journal of Geophysical Research: Atmospheres*, 107(D18), AAC 3-1-
 996 AAC 3-21. <https://doi.org/https://doi.org/10.1029/2001JD000970>
- 997 Schill, G. P., Froyd, K. D., Bian, H., Kupc, A., Williamson, C., Brock, C. A., Ray, E., Hornbrook, R. S.,
 998 Hills, A. J., Apel, E. C., Chin, M., Colarco, P. R., & Murphy, D. M. (2020). Widespread biomass
 999 burning smoke throughout the remote troposphere. *Nature Geoscience*, 13(6), 422–427.
 1000 <https://doi.org/10.1038/s41561-020-0586-1>
- 1001 Shen, H., Peters, T. M., Casuccio, G. S., Lersch, T. L., West, R. R., Kumar, A., Kumar, N., & Ault, A. P.
 1002 (2016). Elevated Concentrations of Lead in Particulate Matter on the Neighborhood-Scale in Delhi,
 1003 India As Determined by Single Particle Analysis. *Environmental Science & Technology*, 50(10),
 1004 4961–4970. <https://doi.org/10.1021/acs.est.5b06202>
- 1005 Sobanska, S., Coeur, C., Maenhaut, W., & Adams, F. (2003). SEM-EDX Characterisation of
 1006 Tropospheric Aerosols in the Negev Desert (Israel). *Journal of Atmospheric Chemistry*, 44(3), 299–
 1007 322. <https://doi.org/10.1023/A:1022969302107>
- 1008 Sobanska, S., Falgayrac, G., Rimetz-Planchon, J., Perdrix, E., Brémard, C., & Barbillat, J. (2014).
 1009 Resolving the internal structure of individual atmospheric aerosol particle by the combination of
 1010 Atomic Force Microscopy, ESEM–EDX, Raman and ToF–SIMS imaging. *Microchemical Journal*,
 1011 114, 89–98. <https://doi.org/https://doi.org/10.1016/j.microc.2013.12.007>
- 1012 Sorooshian, A., Corral, A. F., Braun, R. A., Cairns, B., Crosbie, E., Ferrare, R., Hair, J., Kleb, M. M.,
 1013 Hossein Mardi, A., Maring, H., McComiskey, A., Moore, R., Painemal, D., Scarino, A. J.,
 1014 Schlosser, J., Shingler, T., Shook, M., Wang, H., Zeng, X., ... Zuidema, P. (2020). Atmospheric
 1015 Research Over the Western North Atlantic Ocean Region and North American East Coast: A
 1016 Review of Past Work and Challenges Ahead. *Journal of Geophysical Research: Atmospheres*,
 1017 125(6), e2019JD031626. <https://doi.org/https://doi.org/10.1029/2019JD031626>
- 1018 Spracklen, D. v, Carslaw, K. S., Pöschl, U., Rap, A., & Forster, P. M. (2011). Global cloud condensation
 1019 nuclei influenced by carbonaceous combustion aerosol. *Atmospheric Chemistry and Physics*, 11(17),
 1020 9067–9087. <https://doi.org/10.5194/acp-11-9067-2011>

- 1021 Stein, A. F., Draxler, R. R., Rolph, G. D., Stunder, B. J. B., Cohen, M. D., & Ngan, F. (2015). NOAA's
 1022 HYSPLIT Atmospheric Transport and Dispersion Modeling System. *Bulletin of the American*
 1023 *Meteorological Society*, *96*(12), 2059–2077. <https://doi.org/10.1175/BAMS-D-14-00110.1>
- 1024 Stevens, B., Bony, S., Farrell, D., Ament, F., Blyth, A., Fairall, C., Karstensen, J., Quinn, P. K., Speich,
 1025 S., Acquistapace, C., Aemisegger, F., Albright, A. L., Bellenger, H., Bodenschatz, E., Caesar, K.-A.,
 1026 Chewitt-Lucas, R., de Boer, G., Delanoë, J., Denby, L., ... Zöger, M. (2021). EUREC4A. *Earth*
 1027 *Syst. Sci. Data*, *13*(8), 4067–4119. <https://doi.org/10.5194/essd-13-4067-2021>
- 1028 Stevens, B., Farrell, D., Hirsch, L., Jansen, F., Nuijens, L., Serikov, I., Brüggemann, B., Forde, M., Linne,
 1029 H., Lonitz, K., & Prospero, J. M. (2016). The Barbados Cloud Observatory: Anchoring
 1030 Investigations of Clouds and Circulation on the Edge of the ITCZ. *Bulletin of the American*
 1031 *Meteorological Society*, *97*(5), 787–801. <https://doi.org/10.1175/BAMS-D-14-00247.1>
- 1032 Talbot, R. W., Andreae, M. O., Berresheim, H., Artaxo, P., Garstang, M., Harriss, R. C., Beecher, K. M.,
 1033 & Li, S. M. (1990). Aerosol chemistry during the wet season in central Amazonia: The influence of
 1034 long-range transport. *Journal of Geophysical Research: Atmospheres*, *95*(D10), 16955–16969.
 1035 <https://doi.org/https://doi.org/10.1029/JD095iD10p16955>
- 1036 Tomlin, J. M., Jankowski, K. A., Veghte, D. P., China, S., Wang, P., Fraund, M., Weis, J., Zheng, G.,
 1037 Wang, Y., Rivera-Adorno, F., Raveh-Rubin, S., Knopf, D. A., Wang, J., Gilles, M. K., Moffet, R.
 1038 C., & Laskin, A. (2021). Impact of dry intrusion events on the composition and mixing state of
 1039 particles during the winter Aerosol and Cloud Experiment in the Eastern North Atlantic (ACE-
 1040 ENA). *Atmospheric Chemistry and Physics*, *21*(24), 18123–18146. [https://doi.org/10.5194/acp-21-](https://doi.org/10.5194/acp-21-18123-2021)
 1041 [18123-2021](https://doi.org/10.5194/acp-21-18123-2021)
- 1042 Tsamalis, C., Chédin, A., Pelon, J., & Capelle, V. (2013). The seasonal vertical distribution of the
 1043 Saharan Air Layer and its modulation by the wind. *Atmos. Chem. Phys.*, *13*(22), 11235–11257.
 1044 <https://doi.org/10.5194/acp-13-11235-2013>
- 1045 Twohy, C. H., Kreidenweis, S. M., Eidhammer, T., Browell, E. v., Heymsfield, A. J., Bansemer, A. R.,
 1046 Anderson, B. E., Chen, G., Ismail, S., DeMott, P. J., & van den Heever, S. C. (2009). Saharan dust
 1047 particles nucleate droplets in eastern Atlantic clouds. *Geophysical Research Letters*.
 1048 <https://doi.org/10.1029/2008GL035846>
- 1049 Twomey, S. (1974). Pollution and the planetary albedo. *Atmospheric Environment (1967)*, *8*(12), 1251–
 1050 1256. [https://doi.org/https://doi.org/10.1016/0004-6981\(74\)90004-3](https://doi.org/https://doi.org/10.1016/0004-6981(74)90004-3)
- 1051 Twomey, S. (1977). The Influence of Pollution on the Shortwave Albedo of Clouds. *Journal of*
 1052 *Atmospheric Sciences*, *34*(7), 1149–1152. [https://doi.org/10.1175/1520-](https://doi.org/10.1175/1520-0469(1977)034<1149:TIOPOT>2.0.CO;2)
 1053 [0469\(1977\)034<1149:TIOPOT>2.0.CO;2](https://doi.org/10.1175/1520-0469(1977)034<1149:TIOPOT>2.0.CO;2)
- 1054 Wang, Q., Saturno, J., Chi, X., Walter, D., Lavric, J. v, Moran-Zuloaga, D., Ditas, F., Pöhlker, C., Brito,
 1055 J., Carbone, S., Artaxo, P., & Andreae, M. O. (2016). Modeling investigation of light-absorbing
 1056 aerosols in the Amazon Basin during the wet season. *Atmospheric Chemistry and Physics*, *16*(22),
 1057 14775–14794. <https://doi.org/10.5194/acp-16-14775-2016>
- 1058 Wex, H., Dieckmann, K., Roberts, G. C., Conrath, T., Izaguirre, M. A., Hartmann, S., Herenz, P., Schäfer,
 1059 M., Ditas, F., Schmeissner, T., Henning, S., Wehner, B., Siebert, H., & Stratmann, F. (2016).
 1060 Aerosol arriving on the Caribbean island of Barbados: physical properties and origin. *Atmos. Chem.*
 1061 *Phys.*, *16*(22), 14107–14130. <https://doi.org/10.5194/acp-16-14107-2016>

- 1062 Wu, H., Taylor, J. W., Langridge, J. M., Yu, C., Allan, J. D., Szpek, K., Cotterell, M. I., Williams, P. I.,
1063 Flynn, M., Barker, P., Fox, C., Allen, G., Lee, J., & Coe, H. (2021). Rapid transformation of
1064 ambient absorbing aerosols from West African biomass burning. *Atmospheric Chemistry and
1065 Physics*, 21(12), 9417–9440. <https://doi.org/10.5194/acp-21-9417-2021>
- 1066 Yu, H., Tan, Q., Chin, M., Remer, L. A., Kahn, R. A., Bian, H., Kim, D., Zhang, Z., Yuan, T., Omar, A.
1067 H., Winker, D. M., Levy, R., Kalashnikova, O., Crepeau, L., Capelle, V., & Chedin, A. (2019).
1068 Estimates of African Dust Deposition Along the Trans-Atlantic Transit Using the Decade-long
1069 Record of Aerosol Measurements from CALIOP, MODIS, MISR, and IASI. *Journal of Geophysical
1070 Research. Atmospheres : JGR*, 124(14), 7975–7996. <https://doi.org/10.1029/2019JD030574>
- 1071 Zauscher, M. D., Wang, Y., Moore, M. J. K., Gaston, C. J., & Prather, K. A. (2013). Air Quality Impact
1072 and Physicochemical Aging of Biomass Burning Aerosols during the 2007 San Diego Wildfires.
1073 *Environmental Science & Technology*, 47(14), 7633–7643. <https://doi.org/10.1021/es4004137>
- 1074 Zhang, R., Khalizov, A. F., Pagels, J., Zhang, D., Xue, H., & McMurry, P. H. (2008). Variability in
1075 morphology, hygroscopicity, and optical properties of soot aerosols during atmospheric processing.
1076 *Proceedings of the National Academy of Sciences*, 105(30), 10291–10296.
1077 <https://doi.org/10.1073/pnas.0804860105>
- 1078 Zuidema, P., Alvarez, C., Kramer, S. J., Custals, L., Izaguirre, M., Sealy, P., Prospero, J. M., & Blades, E.
1079 (2019). Is Summer African Dust Arriving Earlier to Barbados? The Updated Long-Term In Situ
1080 Dust Mass Concentration Time Series from Ragged Point, Barbados, and Miami, Florida. *Bulletin of
1081 the American Meteorological Society*, 100(10), 1981–1986. [https://doi.org/10.1175/BAMS-D-18-
0083.1](https://doi.org/10.1175/BAMS-D-18-
1082 0083.1)
- 1083 Zuidema, P., Sedlacek III, A. J., Flynn, C., Springston, S., Delgadillo, R., Zhang, J., Aiken, A. C.,
1084 Koontz, A., & Muradyan, P. (2018). The Ascension Island Boundary Layer in the Remote Southeast
1085 Atlantic is Often Smoky. *Geophysical Research Letters*, 45(9), 4456–4465.
1086 <https://doi.org/https://doi.org/10.1002/2017GL076926>
- 1087 Zuidema, P., Xue, H., & Feingold, G. (2008). Shortwave Radiative Impacts from Aerosol Effects on
1088 Marine Shallow Cumuli. *Journal of the Atmospheric Sciences*, 65(6), 1979–1990.
1089 <https://doi.org/10.1175/2007JAS2447.1>
- 1090
- 1091